Characterization of Lipid Deposition on Contact Lenses

by

Han Qiao

A thesis
presented to the University of Waterloo
in fulfillment of the
thesis requirement for the degree of
Master of Science
in
Vision Science

Waterloo, Ontario, Canada, 2017

Author's Declaration

I hereby declare that I am the sole author of this thesis. This is a true copy of the thesis, including any required final revisions, as accepted by my examiners.

I understand that my thesis may be made electronically available to the public.

Abstract

Purpose

The purpose of this thesis was to evaluate the influence of lipid deposition on silicone hydrogel contact lens materials and to construct an *in vitro* platform to further explore the effect of lipid interaction with contact lenses under physiologically relevant conditions.

Methods

In Chapter 3, the location of fluorescently tagged cholesteryl ester deposition was evaluated on four silicone hydrogel lens materials after simulated contact lens wear with a vial model for 1 day, 14 days and 30 days, using a CLSM technique.

In Chapter 4, the design and implementation of a blink mechanism on an *in vitro* eye model was outlined.

In Chapter 5, the design and implementation of a tear film onto an *in vitro* eye model was outlined.

In Chapter 6, the non-invasive tear film break-up time of two silicone hydrogels were evaluated after simulated contact lens wear with an *in vitro* eye model.

In Chapter 7, the limitations and future directions of the *in vitro* eye model was outlined.

Results

Overall, the amount of accumulated cholesteryl ester in silicone hydrogels increased with prolonged incubation periods. The level of surface versus bulk cholesteryl ester deposition varied with lens material depending upon their surface and bulk properties.

A blink mechanism and tear film structure were established on the *in vitro* eye model, allowing

physiological simulations of tear volume, tear flow, intermittent air exposure, and mechanical wear.

Non-invasive tear break-up time of the pre-lens tear film on silicone hydrogels was successfully measured for lotrafilcon B, which presented values that were comparable to clinical tear break-up times.

Conclusion

This thesis reported a complex relationship between lipid deposition on silicone hydrogels and detailed the developments of a physiologically relevant *in vitro* eye model to move towards a better understanding of the effect of lipid deposition on contact lens discomfort.

Acknowledgements

I owe my deepest gratitude to my supervisors, Lyndon Jones and Lakshman Subbaraman, for their endless support and unwavering dedication.

I would like to acknowledge my committee members, Gina Sorbara and Denise Hileeto for their invaluable guidance.

Additionally, I wish to extent my appreciation to the rest of the CCLR family, graduate students and optometry faculty, who have all helped make this thesis a reality.

Dedication

This thesis is dedicated to my lovely mother and David Liu.

Table of Contents

List of Figures

List of Tables

List of Symbols and Abbreviations

ABS	acrylonitrile butadiene styrene
ATS	artificial tear solution
BUT	break-up time
CCLR	centre for contact lens research
CE	cholesteryl ester
CE-NBD	5-cholesten-3ß-ol 6-[(7-nitro-2-1,3-benzoxadiazol-4-yl)amino]caproate
CL	contact lens
CLSM	confocal laser scanning microscopy
CO	cholesteryl oleate
CSS	complex salt solution
Dk	oxygen permeability
Dk/t	oxygen transmissibility
DL	digital materials
FDM	fuse deposition modeling
MBC	model blink cell
NIBUT	non-invasive tear break-up time
PBS	phosphate buffer saline
PDMS	polydimethylsiloxane
PMMA	polymethylmethacrylate
pHEMA	poly-2-hydroxyethyl methacrylate
PVA	polyvinyl alcohol
RIF	relative intensity fluorescence
SLA	stereo lithography
SLS	selective laser sintering

Chapter 1 – Introduction

1.1 Contact Lenses

The concept of a contact lens (CL) was first introduced by Leonardo da Vinci, when he altered the refractive power of the eye using optical contact with water in 1508.[1] However, it was not until 1888 that a CL was manufactured and fitted in the form of glass scleral lenses.[2] Unfortunately, these lenses were not widely adopted because they were uncomfortable to wear for extended periods and were impermeable to oxygen. Since then, many iterations of CLs have been developed, with the intent to continually improve comfort and safety. A major factor driving these changes was the development of specialized plastic materials that could be manufactured as CLs, most notably polymethylmethacrylate (PMMA) and poly-2-hydroxyethyl methacrylate (pHEMA). Today, CLs have become an important medical device with increasing popularity as the need for vision correction continues to rise. With an estimated more than 140 million CL wearers worldwide,[3] the most prescribed lenses today are soft hydrogels, which can be classified into conventional hydrogels and silicone hydrogels.[4, 5]

1.1.1 Conventional Hydrogels

Developed in the early 1960s, the invention of pHEMA polymers revolutionized CL fitting due to their superior comfort.[2] Unlike its predecessor, rigid lenses made from PMMA, conventional hydrogels made from pHEMA were soft and flexible under hydrated conditions.[2] In addition, conventional hydrogels were hydrophilic, allowing for absorption and retention of high water content in the lens.[2, 6] Initially, these hydrogel lenses were manufactured by Wichterle using a spin casting method.[2, 7] It was not until Bausch & Lomb purchased Wichterle's patent and began mass production that soft lenses gained significant popularity.[2, 7]

Despite its success in the CL market, a shortcoming of hydrogel materials is the lack of oxygen delivery to the eye during lens wear, particularly when worn overnight. The amount of oxygen received by the eye is primarily dependent on the amount of oxygen dissolved in the water phase that hydrates the lens. Oxygen transmissibility through the lens is described by the term Dk/t, where Dk is the oxygen permeability of the lens material and t is the lens thickness. Due to the inherent low Dk of pHEMA, conventional hydrogels do not provide sufficient oxygen required for extended or overnight lens wear.[8, 9] Hypoxic exposure of the cornea puts lens wearers at greater risks of complications such as neovascularization, infectious keratitis, altered endothelial morphology and reduced corneal function.[10-12] To address these issues, a new era of CLs were launched into the market.

1.1.2 Silicone Hydrogels

The first attempt at incorporating an oxygen-loving backbone, silicone elastomer, into a CL dates back to the 1970s. While silicone elastomers enabled exceptional oxygen transmissibility of the lens and significantly reduced the levels of overnight corneal edema,[13] the hydrophobic nature of the lens material failed to retain the necessary water content for comfort.[14] It was not until the 1990s that Bausch & Lomb and CIBA Vision launched the first generation of silicone hydrogels, PureVision (balafilcon A) and Focus Night & Day (lotrafilcon A). Unlike the silicone elastomeric lenses, silicone hydrogels incorporated siloxane monomers that provided enhanced oxygen transmissibility, while maintaining the ability to retain a reasonably high water content.[15, 16] The wettability of PureVision and Focus Night & Day was greatly increased by disguising the hydrophobic domains of silicone monomers through surface treatments. PureVision's hydrophilic silicate surface was created by a plasma oxidation process, whereas Focus Night & Day obtained a 25 nm hydrophilic plasma coating on both the front and back surfaces of the lens. More than a decade later, a second generation of silicone hydrogels were produced, with the introduction of Acuvue Advance (galyfilcon A) and then

Acuvue Oasys (senofilcon A) by Johnson & Johnson. These lenses did not require a surface treatment process to maintain wettability, but had improved wettability through the incorporation of an internal wetting agent, polyvinylpyrollidone. Shortly after, CooperVision released the third generation silicone hydrogels, marketed as Biofinity (comfilcon A). By taking advantage of inherently wettable materials, no surface treatment or wetting agents were required to maintain hydration within Biofinity. More recently, Alcon released Dailies Total1 (delefilcon A), which integrates a silicone core with a non-silicone hydrophilic surface to meet both the oxygen and hydration demand of the lens. Despite the considerable advancements made to increase the wettability of silicone hydrogels, CL discomfort remains an unsolved issue.

1.2 Tear Film

CL discomfort is a complex subject due to the multifactorial influences at play. Particularly, one of the key contributing elements is CL deposits. These deposits originate from the tear film, which serves to lubricate the anterior surface of the eye, provide nutrients to the cornea and conjunctiva, protect the cornea from foreign particles, and maintain an optically smooth surface for unhindered vision.[17] The tear film is approximately 3-7 μm thick and 3-6.2 μL in volume.[18-21] Initially proposed by Wolff,[22] the tear film is made up of three distinct layers: a superficial lipid layer, a middle aqueous layer, and an inner mucin layer. More recent research on the tear film has challenged the trilayered structure and instead suggested a bilayered structure, consisting of an aqueous phase with increasing mucin concentrations towards the corneal epithelial and a distinct outer lipid phase.[20, 23] Each of these layers play an integral role in maintaining the structural integrity and functionality of the tear film.

1.2.1 Aqueous Mucin Layer

In this section, the bilayered tear film structure will be described. The aqueous mucin layer makes up the bulk of the tear film and contains various mucins, electrolytes and proteins bathed in water. The electrolytes regulate the pH and osmolarity of tears,[24] whereas the mucins and proteins play a key role in defending the eye against viral and bacterial infections.[24, 25] While most of the aqueous component is secreted by the lacrimal gland, mucins are secreted by the goblet cells of the conjunctiva. Some of these mucins adhere to the anterior surface of the eye to establish a hydrophilic interphase, while others interact with the aqueous phase to generate a continuous tear film structure.[26, 27]

Amongst the 1500 different tear proteins that have been identified in the aqueous layer, lysozyme, lactoferrin, immunoglobulin and albumin are found in the highest concentrations in the tear film.[28-31] Each protein functions uniquely to prevent microbial infections. Lysozyme (14 kDa) functions as an antibacterial agent by cleaving the peptidoglycan of bacterial cells. Lactoferrin (82 kDa) reduces the susceptibility of bacterial infections by binding to free iron in the tears to effectively limiting the necessary iron available for microbial growth.[32, 33] Immunoglobulins (450 kDa) passively prevent the adhesion of microorganisms and actively induces phagocytosis upon binding to bacteria.[34] Although albumin (66 kDa) in the blood has been extensively studied and associated with various functions, the role of albumin in tears remains unclear.[35]

1.2.2 Lipid Layer

The lipid layer is composed of mostly secretions from the meibomian gland, which are modified sebaceous glands arranged in parallel rows within the tarsal plate of the eyelids. On average, each eye has approximately 30-40 glands in the upper lid and 20-30 glands in the lower lid.[36] Each gland ranges from 2-5.5 mm in length and comprises of 10-15 lipid producing acini.[36, 37] With the

movement and pressure generated from a blink, the lipids within the acini are secreted onto the eye in small amounts through the meibomian gland orifices along the lid margin. The secreted lipids spread evenly over the aqueous layer to form an approximately 0.1 μm thick lipid layer.[38] This thin layer prevents evaporation of the aqueous phase, provides an ocular lubricant to enable a smooth blink, and acts as a protective barrier against foreign particles.[39]

The lipid layer can be further broken down into an inner polar or amphiphilic phase (30%) and an outer nonpolar phase (70%).[39] The polar phase primarily consists of lipids such as phospholipids and glycolipids.[40, 41] These lipids are amphiphilic, which allow the hydrophilic polar head group to network with the aqueous layer and the hydrophobic fatty acid tail to interact with the outer nonpolar phase that is exposed to the air. The nonpolar phase is composed of cholesteryl esters, wax esters, free cholesterol, hydrocarbons and triglycerides.[42-44] Although all of the polar and nonpolar lipids play an important role in the tear film integrity and function, the lipid of interest in this thesis is cholesteryl ester, which is found in an abundant amount on the lipid layer.[44]

Cholesteryl ester is a class of cholesterols with an ester bond attached to hydrocarbon chains of various lengths (Figure 1-1).[45] Previously, researchers have found that large quantities of hydrophobic chains from cholesteryl esters allow for the self-assembly of liquid-crystal-like structures that can be modulated by varying interaction with other molecules.[45] Hence, the presence of cholesterol is believed to be vital in maintaining the structural integrity of the tear film.[46]

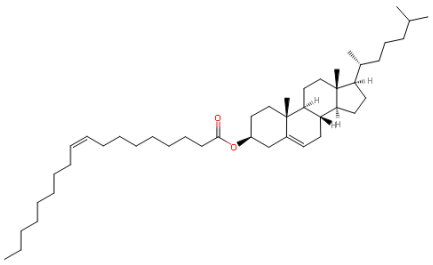

Figure 1-1. Chemical structure of cholesteryl oleate (a cholesteryl ester).

However, the insertion of a CL onto the eye drastically influences the intricate structure and function of the tear film. The structure is split into a pre-lens and post-lens tear film, effectively decreasing the pre-lens tear film thickness.[47] These changes have a significant impact on the ocular surface as well as the CL. Notably, tear film components are known to deposit onto the CL, changing the lens property and affecting the comfort experienced by the lens wearer.[48-50]

1.3 Contact Lens Deposition

Generally, deposits on the CL are seen as unfavourable as they can affect visual acuity, promote bacterial adhesion, and cause symptoms of dryness and discomfort.[48, 49, 51] The two major deposits found on CL materials are proteins and lipids from the tear film. Proteins are known to accumulate in large amounts on conventional hydrogels, mainly due to its affinity to the ionic charges from the lens polymers.[52-59] Therefore, positively charged proteins such as lysozyme and lactoferrin have been shown to deposit in high amounts to negatively charged hydrogel materials.[58-61] Whereas, a lower concentration of negatively charged albumin are found to deposit on the lens.[62] In addition to the quantity of protein deposits, the conformational state of proteins upon depositing in the lens also play a role in affecting CL discomfort and may induce papillary conjunctivitis.[63-68]

1.3.1 Lipid Deposition in Conventional Hydrogels

Hart et al. were among the first to observe “jelly-bump” deposits, composed mainly of

cholesteryl esters and triglycerides, on extended-wear conventional hydrogel lenses.[69] A suggested mechanism for these deposits was the local depletion of aqueous tear layer over the surface of the CL, which created a dry spot for lipid accumulation.[69] Due to the insolubility of lipids in aqueous solutions, these deposits exhibited resistance to cleaning regimes.[69] Moreover, heavy depositors were correlated to a decreased tear flow and higher tear lipid levels.[69] To better understand this phenomenon, Tighe et al. used a light scanning electron microscopy technique to characterize the location and morphology of lipid deposits on spoilt conventional lenses.[70] The location of these deposits were consistent irrespective of patient variability, wear schedule and lens type.[70] In addition, a three-layered structure was discovered, with the primary basal layer composed of unsaturated lipids, and the secondary and tertiary layers composed of mostly cholesterol and cholesteryl esters.[70] Primarily, their studies suggested that the basal layer lipids may play a role in altering the surface of the lens and causing reduced biocompatibility.[70]

In addition to surface deposits, lipids were also absorbed into the lens matrix of conventional hydrogels.[71] The lipid composition of patient worn conventional hydrogels was examined by Rapp et al. using various chromatography techniques.[72] The analyses revealed the presence of wax esters, fatty sterols, fatty alcohols and free fatty acids, as well as the absence of triglycerides, cholesterol, and cholesteryl esters.[72] In summary, a higher level of polar lipids deposited in conventional hydrogels compared to nonpolar lipids.[72] Unlike surface deposits, the quantity and quality of lipid deposits in the lens matrix were more sensitive to patient variability, wear schedule and lens type.[71, 73] One study showed considerable variation between subjects and an overall reduction in lipid accumulation in conventional hydrogel lenses worn for a 1 month compared to 3 months.[74] In another study, increased lipid deposition was found in lenses containing NVP.[75, 76]

1.3.2 Lipid Deposition in Silicone Hydrogels

Although lipids accumulate in both conventional and silicone hydrogels, they deposit significantly more on silicone hydrogels due to their inherent hydrophobic silicate components.[77-79] With the increasing popularity of silicone hydrogels, lipid deposition studies are becoming more relevant.

The first lipid deposition study with silicone hydrogels was conducted by Jones et al. where the amount and type of lipids deposited in worn conventional and silicone hydrogels were analyzed.[57] Results showed that lipid deposited substantially more in silicone hydrogels than in conventional hydrogels.[57] The lipids that deposited in the highest concentrations were oleic acid, oleic acid methyl ester, and cholesterol.[57] In addition, the amount and type of lipids deposited in silicone hydrogels varied depending on lens properties.[57] Several other studies further confirmed the results from Jones et al., where high levels of lipid deposits were observed in silicone hydrogels.[77, 80-83]

Besides characterizing the amount and type of deposits, researchers also explored other factors that may influence lipid deposition, such as changes in lens wettability, difference in cleaning regimes and its effect on microbial contamination. A study conducted by Lorentz et al. concluded that initial exposure to lipids may improve the wettability of surface treated silicone hydrogels,[84] which may help to explain that comfort tended to increase with these lenses over the first few hours of wear, as lipid deposition increased and wettability improved .[85] In terms of cleaning regimes, several groups have found significantly less lipid accumulation in silicone hydrogels that were cleaned with OptiFree RepleniSH and Aquify.[86-88] In terms of microbial interaction, Babaei Omali et al. showed that the presence of cholesterol on silicone hydrogels did not play a role in modulating bacterial adhesion on the lens surface.[89]

To date, very few studies have directly evaluated the clinical performance of silicone hydrogel

lenses in relation to lipid deposition.[90-92] A study conducted by Cheung et al showed no correlation between the amount of lipid deposits and its effects on visual acuity, corneal integrity, and reported comfort levels.[90] Later, Zhao et al. showed a weak correlation between the amount of cholesterol deposition on silicone hydrogels and adverse effects of CL wear.[91] Evidence linking lipid deposition with CL comfort is either non-existent or weak, although one study conducted by Subbaraman et al. showed that lipid deposition is higher in asymptomatic CL wearers.[92]

Although lipid deposition conducted *in vivo* offer valuable insights with clinical relevance, data interpretation from these studies can become convoluted as a result of intersubject variability, in addition to the complex nature of the CL deposits.[73, 75] Specifically, in a study conducted by Hart et al. evaluating the effect of lifestyle choices on lipid deposition, varying amounts of lipid deposits were seen in patients with various systemic diseases and their level of consumption in protein, alcohol, and cholesterol.[93] The ability to isolate contributing factors involved in CL deposition can allow for simpler analysis and a deepened understanding of their effects on CL discomfort. Moving forward, additional work is needed to elucidate the effect of lipid deposition on CLs and the ocular environment. Specifically, the kinetic and location of lipid deposition can be explored using *in vitro* study designs.

1.4 Eye Models

Aside from *in vivo* studies, other CL testing methods include the use of animal models,[94-97] mathematical models,[98, 99] and *in vitro* models.[60, 64, 100-113] All of these models are important and supplement *in vivo* data in unique ways. However, for the scope of this thesis, the focus is on the use of various *in vitro* models in CL deposition studies.

1.4.1 *In Vitro* Models

In vitro models offer the advantage of testing with low cost, high reproducibility, and high-throughput capabilities. More importantly, *in vitro* models allow researchers to isolate and study the variable of interest from the complex multifactorial ocular environment and to conduct such tests ahead of expensive human clinical trials. The majority of *in vitro* CL studies investigating deposition or drug delivery are conducted in vials,[60, 64, 100-105] which is a popular testing method due to its simplicity and convenience. Generally, vial conditions require incubating lenses in a set volume of artificial tear solution (ATS) that is replenished daily to simulate the total amount of daily tear exchange on the eye of approximately 2 mL, projected based on previous studies measuring tear flow rates.[21, 114] However, these conditions differ drastically from on-eye tear conditions, which has a flow rate of approximately 1.2 μL/min.[21] Exposing CL to large amounts of tear fluid at once will have different deposition kinetics compared to exposing the lens to smaller volumes over time. Although the use of vial models remains widespread, many researchers in the field have begun to recognize its limitations. The eye is a complex system with a structured tear film, regulated tear volume, consistent tear flow, intermittent air exposure, and mechanical wear; parameters which all have a drastic impact on the kinetics of CL deposition. The vial model is an oversimplification of the eye and lacks important physiological parameters, making it challenging to justify whether results from these models are clinically relevant. To make up for these shortcomings, researchers have moved towards developing more sophisticated eye models for studying lipid deposition on the lens.

Ali et al. developed a microfluidic device that simulates physiologically relevant tear volume and flow rate to study the drug release kinetics of hydrogels.[111] Results from this study suggested a more constant and slower drug release rate compared to the vial model. Although this system was designed to study drug delivery in CLs, it serves to recognize the importance of mimicking

physiological conditions to accurately characterize release kinetics, which can easily be applied to deposition studies.

To test the effect of air exposure on lipid deposition, Lorentz et al. developed a device called the model blink cell (MBC).[112] As the name suggests, the model simulates intermittent air exposure experienced during the inter-blink period. The MBC consists of six form-fitting Teflon CL holders mounted in an ATS containing trough. The CL holders are installed onto pistons that can move up and down in the trough to cycle the lenses in and out of ATS (exposed to air) at controlled rates. Results from Lorentz's MBC showed higher levels of lipid deposits in CL with air exposure than without, suggesting that lipid deposition kinetics can be impacted by air exposure, which demonstrates the importance of mimicking physiological conditions.

More recently, Peng et al. developed a different MBC with the main objective of mimicking the *in vivo* fouling mechanism of soft CLs.[106] Similar to Lorentz et al.'s MBC, Peng et al.'s MBC also consists of a Teflon CL mold that is placed inside an ATS containing chamber. The blink mechanism is achieved by withdrawing solution from an exit port, which effectively lowers the ATS volume in the chamber and exposes the CL to the air. The uniqueness of Peng et al.'s MBC is the addition of a distinct lipid layer over the ATS, which allowed for simulation of a realistic lipid deposition mechanism as described by Hart et al.[69] Discrete lipid deposits were observed on the surface the CL, accompanied by a gradual lipid penetration into the lens matrix. These results were consistent with those observed on eye, which suggested a promising outcome for the development of *in vitro* eye models that can replace the need for *in vivo* testing.

To combine the different parameters simulated from the previous models onto one system, Phan et al. developed the OcuFlow, an *in vitro* eye model that allows for the simulation of representative tear volume, tear flow, intermittent air exposure and mechanical wear.[113] The OcuFlow

consists of an eye and eyelid piece that are mounted vertically onto a mechanical system, allowing for both a lateral and rotational movement to simulate intermittent air exposure and mechanical wear respectively. Tear volume and tear flow is controlled by an external microfluidic pump. Notably, this model was the first to allow for the CL to be tested in an upright orientation, which may have a drastic effect particularly on deposition studies. Results from lipid deposition studies conducted by our group using the OcuFlow showed more deposits on the surfaces in certain lens types, which differs from the uniform depositions seen in the vial model.[115] This suggests that the additional factors simulated by the OcuFlow may play a vital role in determining how lipid interacts with the CL on the ocular surface.

In summary, lipid deposition studies conducted using more complex *in vitro* eye models provide results that are different from vial studies, but may better mimic *in vivo* results. The development of *in vitro* eye models provides better validation vehicles for CL testing and expands the boundary of future CL technologies.

Chapter 2 – Thesis Rationale

Since the introduction of CLs in the 1960s, reducing the discomfort experienced during lens wear has been one of the leading research topics in the field of vision science.[2, 3] Discomfort associated with CL wear is multifactorial, and CL deposition has been identified as one of the factors that may contribute to CL comfort.[3, 48] Deposition onto the CL is influenced by a multitude of factors, including the ocular environment, lens material, wear modality, and cleaning regimen.[3, 86-88, 105, 116-120] Hence, understanding the impact of these deposits on the ocular surface and the lens property will provide insights on how to improve comfort. Although, protein deposition was studied extensively in the past, recently, more attention has been given to lipid deposition, particularly on silicone hydrogels.[52, 56, 64, 77, 78, 81-83, 88, 105-107, 109, 121-129]

It is hypothesized that bulk deposits are sequestered within the lens matrix whereas surface deposits may interact with the external environment. For example, lipids deposited on the lens surfaces may be more prone to degradation through oxidative processes, which may contribute to downstream pathways leading to discomfort.[130, 131] Although the composition and amount of lipid deposition on the CL has been characterized from both *in vivo* and *in vitro* studies,[77, 78, 81-83, 88, 105, 121, 132] the location of deposition is not fully understood.[106, 107, 109, 110] This missing link is especially critical since clinical studies showed little to no correlation between the amount of lipid deposits and discomfort.[74, 90, 91, 133] This suggests that rather than the amount of lipid deposits, studies should explore the location of lipids deposited in the CL.

The first objective of this thesis was to determine the location of lipid deposits on various silicone hydrogels using a vial model (Chapter 3). An understanding of surface versus bulk lipid deposition on CLs may elucidate possible underlying mechanisms causing discomfort and lead to the

development of improved lens materials.

The second objective was to develop an *in vitro* eye model capable of simulating lipid deposition on the CL under physiologically relevant conditions (Chapters 4 and 5). The tear film structure is disrupted with the insertion of a CL, which impacts how lipids deposit on the lens. In addition, researchers are beginning to recognize the influence of intermittent air exposure and mechanical wear during blinking on discomfort.[112, 117-119]

The last objective was to validate the simulated physiological conditions by measuring pre-lens tear break-up time (Chapter 6).

Chapter 3 – Location of Lipid Deposits on Silicone Hydrogels Evaluated Using a Vial Model

3.1 Introduction

Upon the insertion of a CL, various tear components readily deposit onto the lens.[60, 132, 134-137] These deposits can alter the lens property and its interaction with the ocular surface,[138, 139] which can cause CL discomfort and reduced visual acuity.[66, 91, 140-142] While protein deposition on CL has been extensively investigated in the past,[52, 56, 64, 122-129] studies on lipid deposition are becoming more prevalent due to the increasing popularity of silicone hydrogels in recent years.[77, 78, 81-83, 88, 106, 107, 110, 121, 132] Although *ex vivo* studies are considered the gold standard for assessing CL deposition, the inherent hidden and uncontrolled variables from human subjects may produce contrasting results between different research groups.[3, 77, 79, 143] *In vitro* models allow the researcher to perform experiments with targeted lipids and a controlled experimental setup that is otherwise difficult to achieve *in vivo*. In this study, lipid deposition was explored using an *in vitro* model to simulate CL wear by immersing the lens in ATS.

Currently, most lipid deposition studies examined the quantity of lipid deposits *ex vivo* from whole lens extracts.[77, 78, 81-83, 88, 121, 132] Thus far, limited studies have investigated the location of lipid deposits on the lens.[106-111] Previous studies have visualized surface and bulk lipid deposition using various lipid stains, such as Nile Red and oil red O. However, contrasting results were observed in the stain behavior between different studies[107, 110] and it is suggested that lipid stains may produce inconsistent staining that is not reflective of actual lipid deposits within the lens.[106] Results from other studies observed higher levels of uniform lipid deposition in silicone hydrogels than hydrogels, which may be elucidated due to the continuous hydrophobic silicone microdomains within silicone

hydrogels.[106, 108] However, the pattern of surface versus bulk distribution of lipids and their effect on the CL remains unclear.

To study the location of lipid deposition, fluorescently labelled cholesteryl ester (CE-NBD) was used as a representative tear lipid.[82, 144-147] Structurally, the sterol ring structure of CE was preserved, while the functional group was replaced by a similar sized probe with a comparable molecular weight (Figure 3-1), to allow for unhindered lipid deposition in the CL. In addition, the NBD probe was selected for its high quantum yield, which allows for reliable imaging.

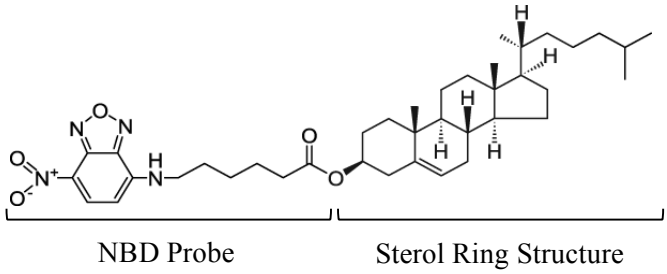

Figure 3-1. Chemical structure of CE-NBD.

The relative distribution of the lipid at various depths within the CL was mapped using confocal laser scanning microscopy (CLSM). What sets CLSM apart from other microscopic techniques is the addition of a spatial pinhole, which eliminates electromagnetic waves that are not in focus on the confocal plane. The pinhole allows for high resolution imaging at different depths into the CL (optical sectioning), through a process known as z-stacking. The purpose of this chapter is to explore the deposition pattern of fluorescently tagged nonpolar lipid over time in silicone hydrogel materials evaluated using CLSM.

3.2 Materials and Methods

3.2.1 Contact Lenses

Four monthly replacement silicone hydrogels (lotrafilcon B [Air Optix® Aqua, Alcon, Fort

Worth, TX], comfilcon A [Biofinity®, CooperVision, Pleasanton, CA], samfilcon A [Ultra®, Bausch + Lomb, Rochester, NY], and senofilcon C [Acuvue® Vita™, Johnson & Johnson, Jacksonville, FL]) were evaluated. All lenses were obtained from the manufacturer in the original packaging and had a dioptric power of -3.00 and the lens properties are outlined in Table 3-1.

Table 3-1. Properties of silicone hydrogels used in the study.

	Acuvue® Vita™	**Air Optix® Aqua**	**Biofinity®**	**Ultra®**
United States Adopted Name (USAN)	senofilcon C	lotrafilcon B	comfilcon A	samfilcon A
Manufacturer	Johnson & Johnson	Alcon	CooperVision	Bausch + Lomb
Centre Thickness (mm)	0.07	0.08	0.08	0.07
Water Content (%)	41	33	48	46
Oxygen Permeability ($x10^{-11}$)	122	110	128	114
Oxygen Transmissibility ($x10^{-9}$)	147	138	160	163
Surface Treatment	None	Plasma Coating	None	None
Wetting Agent	PVP	Moist agent in packaging solution (1% copolymer 845)	None	PVP
Principal Monomers	Not disclosed	DMA + TRIS + siloxane macromer	NVP, VMA, IBM, TAIC, M3U, FM0411M, HOB	Not disclosed

DMA, N,N-dimethylacrylamide; EGDMA, ethyleneglycol dimethacrylate; HEMA, hydroxyethyl methacrylate; MA, methacrylic acid; mPDMS, monofunctional polydimethylsiloxane; NVP, N-vinyl pyrrolidone; TEGDMA, tetraethyleneglycol dimethacrylate; TPVC, tris-(trimethylsiloxysilyl) propylvineyl carbamate; TRIS, trimethylsiloxy silane; NVA – N-vinyl amino acid; PBVC, poly(dimethysiloxy) di(silylbutanol) bis(vineyl carbamate); PC, phosphorylcholine; PVP, polyvinyl pyrrolidone; NVP, *N*-vinyl pyrrolidone; VMA, *N*-vinyl-*N*-methylacetamide; IBM, isobornyl methacrylate; TAIC, 1,3,5-triallyl-1,3,5-triazine-2,4,6(1*H*,3*H*,5*H*)-trione; M3U, bis(methacyloyloxyethyl iminocarboxy ethyloxypropyl)-poly(dimethylsiloxane)-poly(trifluoropropylmehylsiloxane)-poly(methoxy-poly[ethyleneglycol] propylmethlsiloxane); FM0411M, methacryloyloxyethyl iminocarboxyethyloxypropyl-poly(dimethylsiloxy)-butyldimethylsilane; HOB, 2-hydroxybutyl methacrylate.

3.2.2 Artificial Tear Solution

The recipe for ATS used in this study has been previously reported with a few modifications. In brief, the ATS consists of various physiological tear film components, including a range of proteins, lipids and salts (Table 3-2).[148]

Table 3-2. Artificial tear solution components.

Protein Components	mg/mL
Bovine Albumin	0.20
Bovine Submaxillary Mucin	0.15
Bovine Lactoferrin	1.80
Hen Egg Lysozyme	1.90

Lipid Components	mg/mL
Cholesterol	0.00275
Cholesteryl ester NBD	0.00003
Cholesteryl oleate	0.03669
Phosphatidylcholine	0.01116
Phosphatidyethanolamine	0.00592

Salt component	mg/mL
Sodium chloride	5.26
Potassium chloride	1.19
Sodium citrate	0.44
Glucose	0.036
Urea	0.072
Calcium chloride	0.07
Sodium carbonate	1.27
Potassium hydrogen carbonate	0.30
Sodium phosphate dibasic	2.41
Hydrochloric acid	0.94
ProClin 300	0.20 µL / 1 L

In addition, 0.1% of fluorescently-tagged cholesteryl ester (Figure 3-1), 5-cholesten-3ß-ol 6-[(7-nitro-2-1,3-benzoxadiazol-4-yl)amino]caproate (810251P, Avanti Polar Lipids, Inc., Alabaster, AL), was dissolved in ATS.

3.2.3 Experimental Outline

All lenses (n=4) were removed from the original manufacturer's packaging and soaked in 2mL of 1X phosphate buffer saline (PBS) (EMD-Millipore, Billerica, MA) using a 24 well polystyrene plate (Corning®, Corning, NY) to remove residual blister pack solution. After 17 hours of incubation in PBS, CLs were blotted on lens paper to remove any excess PBS held on the lens due to surface tension. Lenses were then transferred to a fresh 24 well plate containing 2 mL of OptiFree®

PureMoist® care solution (Alcon, Fort Worth, TX) to simulate a daily cleaning regime. Plates were sealed using Parafilm (Sigma-Aldrich, St.Louis, MO) and incubated at room temperature for 8 hours. CLs were then removed from OptiFree® PureMoist® care solution. Subsequently, lenses were transferred into a 6 mL vial (Wheaton, Millville, NJ) containing 1mL of ATS for 16 hrs in a 37 °C incubator while rotated at 60 rpm to simulate CL wear. Daily CL wear was simulated for 1 day, 14 days and 30 days by repeating the lens cycling between OptiFree® PureMoist® care solution and ATS on each weekday. Over the weekends, lenses remained incubated in ATS without cycling. Control CLs were incubated in ATS without CE-NBD. To reduce transfer of excess ATS and care solution, all lenses were rinsed in 2 mL of PBS three times after each incubation. After 1 day, 14 days, and 30 days of daily wear simulation in a vial, lenses were removed from ATS and prepared for imaging. CL samples were prepared by punching out a 5 mm disk from the centre of the lens, which was fixed onto a microscope slide (Goldline, VWR, Radnor, PA) for imaging using CLSM.

3.2.4 Confocal Microscopy

The CL samples were imaged using a Zeiss LSM 510 Meta, Axiovert 200 confocal microscope (ZEISS Inc., Toronto, Canada) from the anterior to posterior surface at three randomly selected locations (Figure 3-2.A). To visualize the CE-NBD deposited in the lens, the excitation was set to 488 nm on an Argon laser and the emission wavelength was set to 505 nm using a long pass filter. The CL samples were viewed under a C-Apochromat 40X/1.2 corr objective lens, which magnified the CL such that each visible plane was 224.56 μm^2. A single laser setting could not be used to capture the dynamic range of the fluorescence intensity over four lens types at three incubation time points. To accommodate this, the gain setting on the photomultiplier detector was adjusted accordingly for each lens and incubation period (Table 3-3).

Table 3-3. Gain settings of the photomultiplier detector on the CLSM for different CLs and different incubation times.

Lens	1 day	14 days	30 days
senofilcon C	850	850	700
lotrafilcon B	850	850	775
comfilcon A	800	800	750
samfilcon A	800	800	725

The deposition profile at each plane along the depth of the lens was scanned at 2 µm intervals using z-stacking (Figure 3-2.A) and were rendered into a cross-sectional image of the CL using ZEN Lite software (ZEISS Inc., Germany) (Figure 3-2.B).

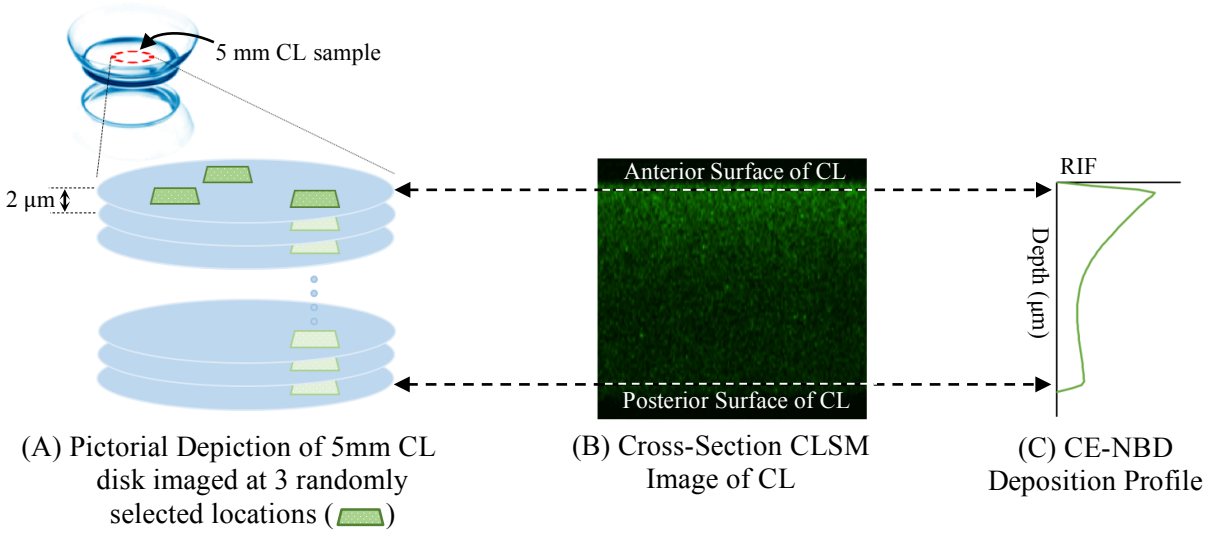

Figure 3-2. Schematic depiction of CLSM imaging and image processing. *Image not to scale.

3.2.5 Image Analysis

The average relative intensity of fluorescence (RIF) value at each plane of the lens was plotted against the depth of the lens using ImageJ software (Bethesda, MS, USA) to graph the corresponding deposition profile curve (Figure 3-2.C). To facilitate the averaging of RIF values between lenses, the

number of planes for each lens was normalized to the equal number of steps (n) using an in-house program that performed piecewise linear interpolation. The program used the first and last data points of the data sequence as the end-points and interpolates $n - 1$ equally spaced steps between the two end points, where 'n' is number of steps determined by the user. After the data sequences were interpolated to the average depth within each lens type, the RIF values imaged at the three locations averaged. The averaged values were then averaged with the four replicates of each lens type. The endogenous fluorescence intensity of the negative control CLs was subtracted from the test CLs. Negative control lenses were imaged at the same confocal settings as those incubated with CE-NBD. To compare the CE-NBD deposition profile between different lens types, the data points were interpolated to $n = 100$ steps and the sequence was normalized to a maximum RIF value of 1 for all lens types. To compare the CE-NBD deposition profiles of the same lens overtime (1 day, 14 days and 30 days) the data points were interpolated to the average depth of the lens and the sequence was normalized to the 30-day maximum RIF of each lens type. In addition, to compare the data between the different incubation periods, a scaling factor was calculated to account for the different gain settings used to capture the images on day 30 (Table 3-3). The scaling factor was achieved by imaging the 14-day CLs at both the 14-day gain setting as well as the 30-day gain setting. The deposition profiles at each gain setting was compared by calculating the area under the curve. The ratio of the area under the curve for both profiles was defined as the scaling factor applied to the 30-day deposition profiles.

3.3 Results

All CLs accumulated CE-NBD over time and the deposition profile varied depending on the duration of incubation and the lens type (Figure 3-3.A-D).

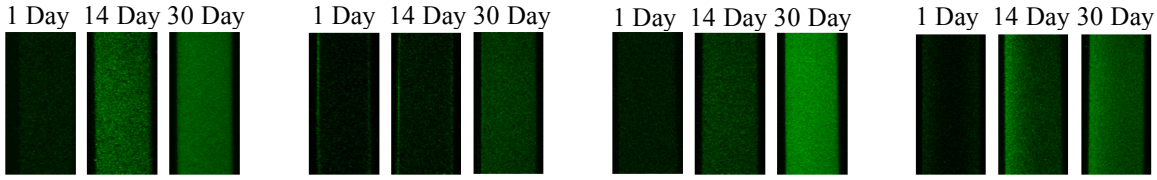

(A) senofilcon C (B) lotrafilcon B (C) comfilcon A (D) samfilcon A

Figure 3-3. Averaged CE-NBD fluoresence images of senofilcon C (A), lotrafilcon B (B), comfilcon A (C), and samfilcon A (D).

3.3.1 Relative Deposition Amount - Within Lens Comparison

To examine the accumulation of CE-NBD over time, the profiles within each lens type at different time points were compared. Generally, a higher RIF value was observed with an increase in incubation period. In senofilcon C (Figure 3-4.A), comfilcon A (Figure 3-4.C), and samfilcon A (Figure 3-4.D), a progressively increasing RIF value was observed in the deposition profiles over time. The increase in RIF value between day 14 and day 30 scaled is higher than between day 1 and day 14. For lotrafilcon B, the RIF value was maintained at the same level between day 1 and day 14, with a significant increase on day-30 (Figure 3-4.B).

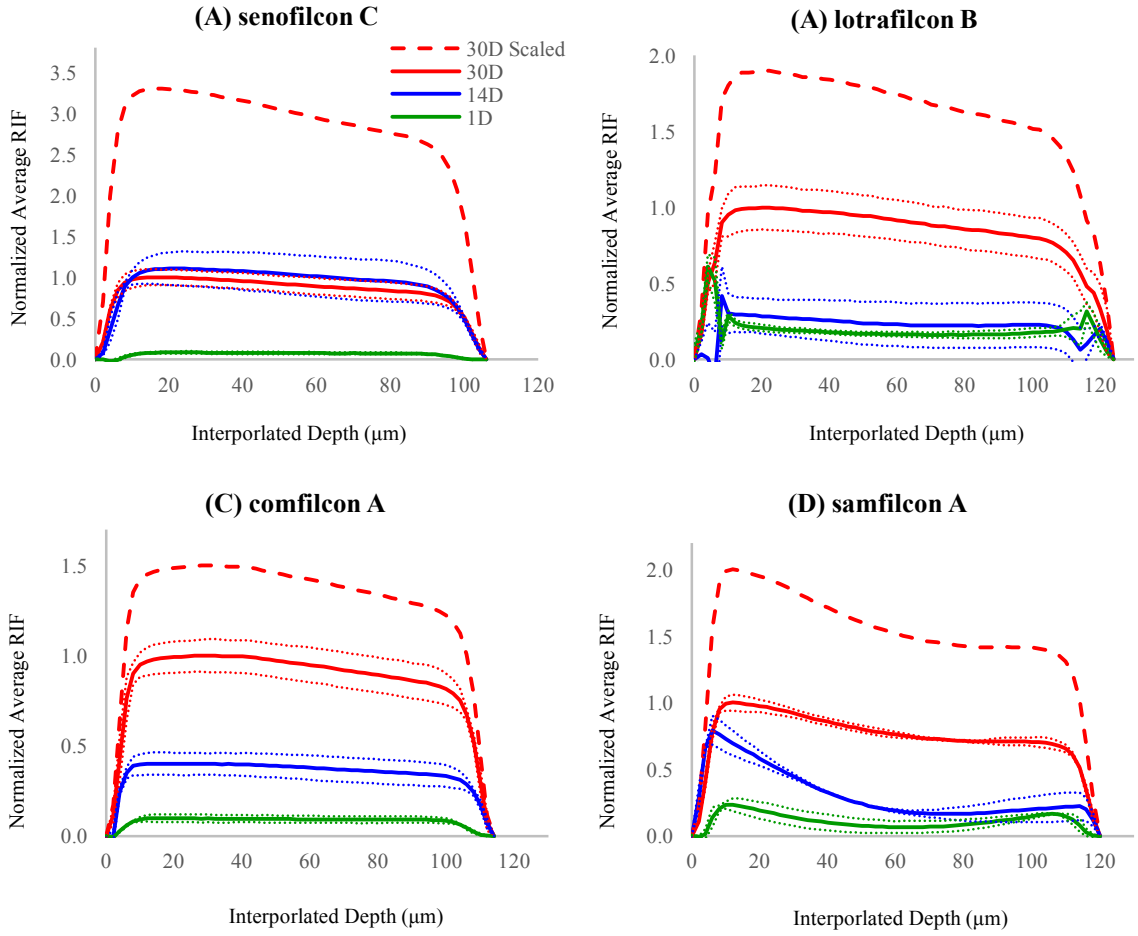

Figure 3-4. CE-NBD deposition profiles of senofilcon C (A), lotrafilcon B (B), comfilcon A (C), samfilcon A (D) lenses plotted at 1 day (———), 14 days (———), and 30 days (———) after incubation in OptiFree® PureMoist® care solution and ATS. The 30-day scaled (– – –) curves were obtained by multiplying the 30-day RIF with a scaling factor of 3.3, 1.9, 1.5, and 2 for senofilcon C, lotrafilcon B, comfilcon A, and samfilcon A respectively. The standard deviation values are shown as dotted lines (·····) in the corresponding colour.

3.3.2 Relative Deposition Pattern - Between Lens Comparison

Between lens types, the deposition profiles were classified into two distinct patterns, a uniform distribution throughout the lens thickness or a surface concentration distribution. After 1 day incubation period (Figure 3-5.A), the deposition profile was uniform in senofilcon C and comfilcon A

materials, whereas lotrafilcon B and samfilcon A had higher RIF values on the surfaces than the core of the lens. In samfilcon A, the RIF value became gradually lower towards the core of the lens. A more extreme deposition profile was observed on lotrafilcon B, where distinct fluorescent peaks were evident on both surfaces with uniformly lower RIF values between the surfaces.

After 14 days incubation period (Figure 3-5.B), senofilcon C and comfilcon A's shapes of the deposition profiles were consistent with results from day 1, where the deposition pattern of CE-NBD was uniform throughout the lens. Although CE-NBD deposition pattern of lotrafilcon B and samfilcon A remained surface concentrated, slight differences were observed at day 14 compared to day 1. For samfilcon A, high RIF values at the front surface of the lens were observed, which gradually decreased towards the core and posterior surface of the lens. For lotrafilcon B, the peaks at both surfaces were less pronounced compared to the level of uniform CE-NBD deposition at the centre of the lens.

After 30 days incubation (Figure 3-5.C), uniform deposition curves suggest that CE-NBD was evenly deposited in all lens types, with the exception of samfilcon A. Although the curve suggests a more homogeneous distribution pattern than at previous incubation periods, samfilcon A maintained a slightly higher RIF value at the front surface after 30 days of incubation.

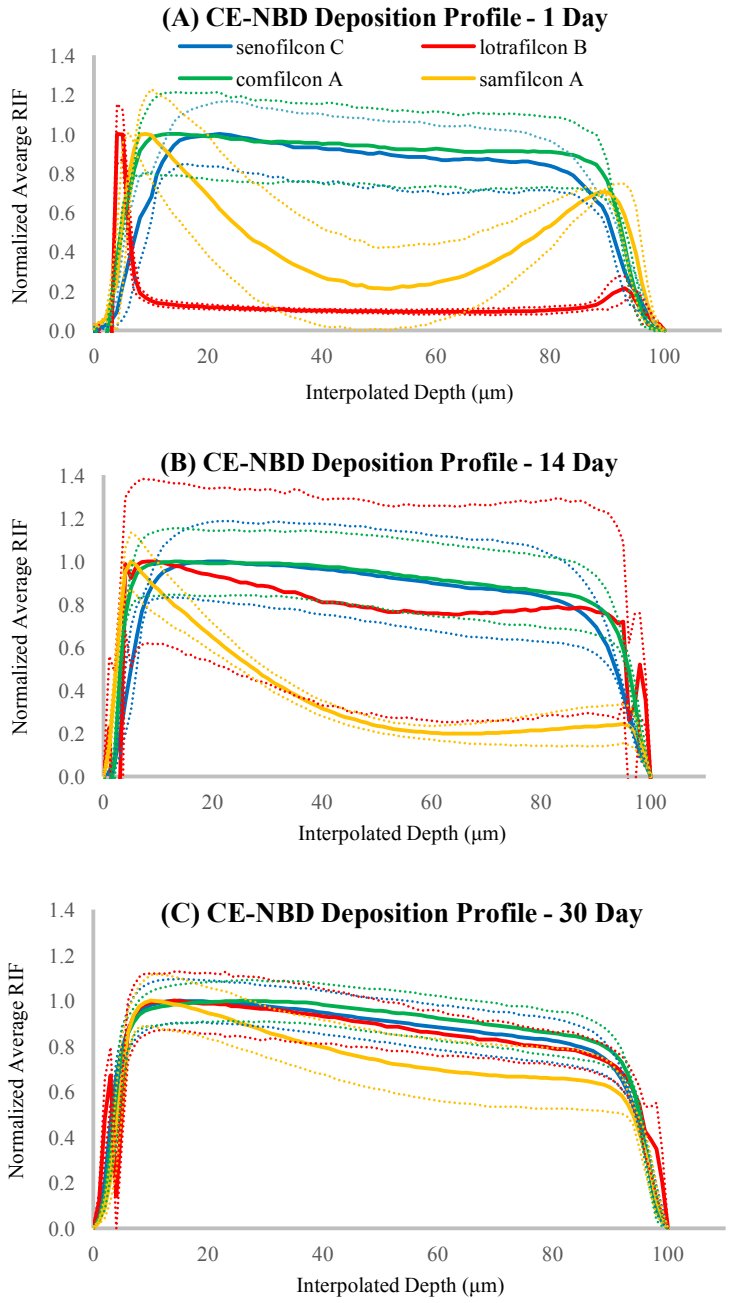

Figure 3-5. Normalized (max of 1) CE-NBD deposition profiles of senofilcon C (———), lotrafilcon B (———), comfilcon A (———), and samfilcon A (———) at 1 day (A), 14 days (B), and 30 days (C) after incubation in OptiFree® PureMoist® care solution and ATS. The standard deviation values are shown as dotted lines (.....) in the corresponding colour.

All CE-NBD deposition profile curves exhibited an apparent asymmetry between the anterior and posterior. To determine the relative asymmetry between the two surfaces, the ratio between the max value on the posterior and anterior surfaces of the lens is plotted in Figure 3-6 after 1 day and 30 days of incubation.

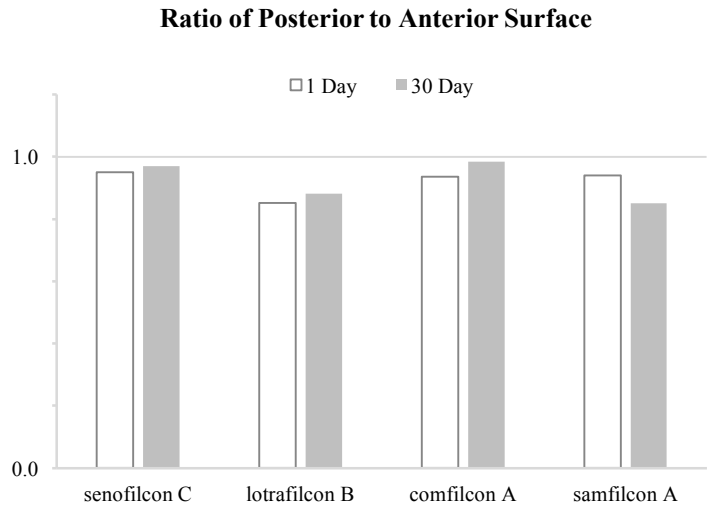

Figure 3-6. Max posterior to max anterior surface RIF ratio of senofilcon C, lotrafilcon B, comfilcon A, and samfilcon A.

The asymmetry phenomenon was most likely due to the attenuation of the fluorescence through the lens with increased distance from the photomultiplier detector. This prediction was verified by an additional set of experiments, which imaged the lenses in the reverse orientation, from the posterior to anterior surface, after 1 day and 30 days of incubation. The reversed CE-NBD deposition profile also showed lower RIF values with increased depth into the CLs at the anterior surface (Figure 3-7), confirming the previous assumption that the asymmetry seen is due to an artifact of the laser, which produces attenuated fluorescence with increased distance away from the photomultiplier detector.

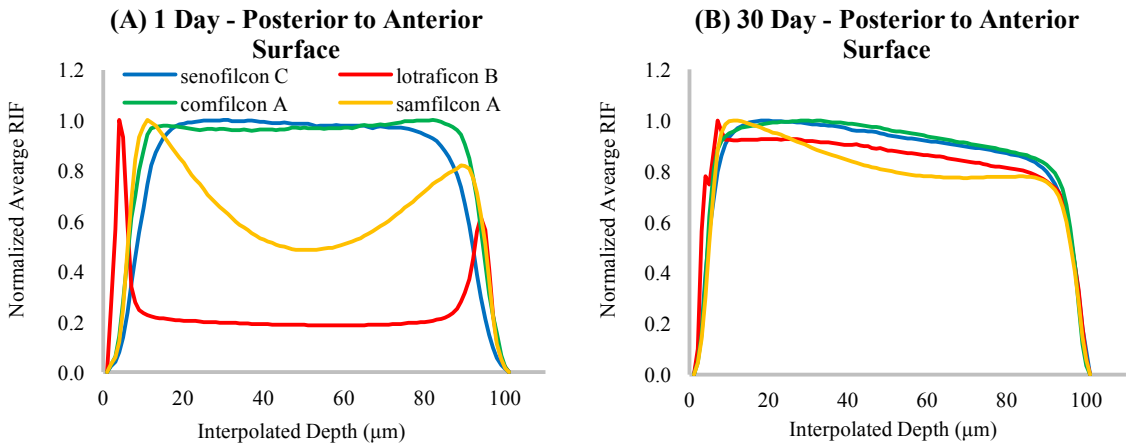

Figure 3-7. CE-NBD deposition profile imaged from the posterior to anterior surface of CLs from 1 Day and 30 Day incubation periods.

The negative control lenses were plotted relative to the test lens in Figure 3-8. With the exception of lotrafilcon B (Figure 3-8.B), all negative control lenses accumulated low background levels of CE-NBD regardless of incubation period. This background signal may be a result of scattering of the laser or endogenous fluorescence of the lens. As a positive control, CLs were incubated in free dye at the molar equivalent of CE-NBD for 1 day and imaged at the same confocal settings. The signals were below negative control levels, suggesting low concentrations of free dye.

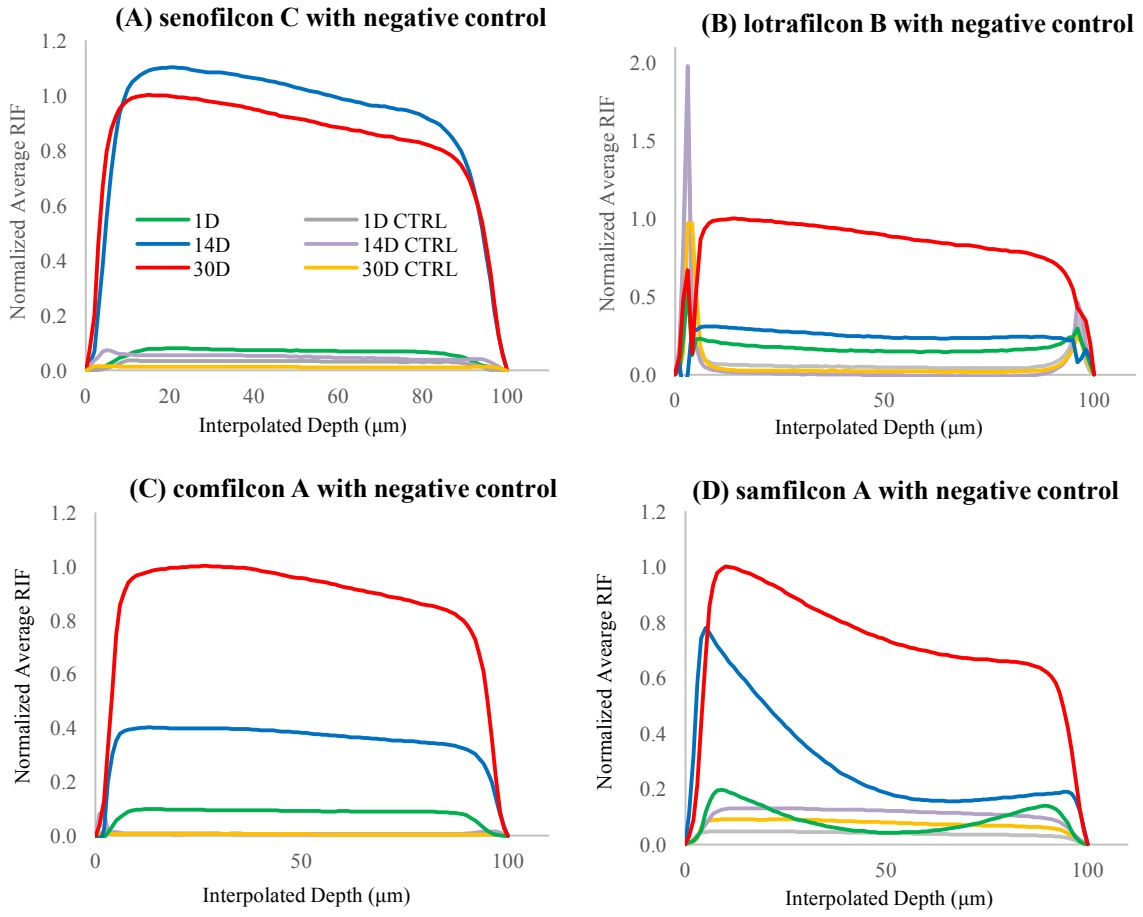

Figure 3-8. CE-NBD deposition profile of senofilcon C (A), lotrafilcon B (B), comfilcon A (C), and samfilcon A (D) plotted with negative controls.

3.4 Discussion

Regardless of lens type, the amount of CE-NBD deposition increased with time, as suggested by an increased RIF value (Figure 3-4). In addition, the increase in CE-NBD deposition between the 14-day and 30-day period is higher than between the first 14 days. Although a cleaning regime was used, lipid deposition continued to increase with time. This progressive increase in the amount of CE-NBD is suspected to be correlated to changes in the lens material over time, such that the lens becomes more susceptible to lipid uptake. Clinically, this progressive increase of lipid deposition in

the CL can be addressed by adopting a daily disposable wear modality.[149]

Overall, two different types of CE-NBD deposition patterns were observed in the CLs. CE-NBD distributed uniformly in senofilcon C and comfilcon A, while the distribution was concentrated on the surfaces in lotrafilcon B and samfilcon A. When the deposition pattern was uniform, the majority of the CE-NBD was effectively accumulated within the core of lens rather than on the surfaces. In comfilcon A, this increased accumulation at the centre of the lens can be explained the presence of N-vinyl pyrrolidone (NVP), which enhances lipid deposition by exposing more hydrophobic surfaces for the lipid to preferentially interact with.[76, 142] Similarly, the high amount of lipid deposition in senofilcon C can be explained by the high levels of PVP wetting agent in the lens, which may result in an increase in lipid solubility.[150] Samfilcon A also incorporates PVP monomers and a more gradual increase in lipid accumulation towards the lens centre was seen in this lens type.

The lotrafilcon B material exhibited the most unique CE-NBD deposition profile. Unlike the other lenses, the RIF value did not increase from day 1 to day 14 (Figure 3-4.B), suggesting that the lens material maintained the same level of CE-NBD over the first 14 days of incubation. This can be explained by the protective effect of the 25 nm plasma treated surface on lotrafilcon B, which reduces the amount of lipid deposition beyond the surfaces.[15, 151] This observation may be correlated to the comparably lower amount of lipid deposited in lotrafilcon B than other CLs seen in previous studies.[57, 82, 121] Moreover, distinct fluorescent peaks were observed on the anterior and posterior surfaces of lotrafilcon B. However, it is unlikely that the peaks resulted from a high accumulation of CE-NBD, since the peaks were also evident in the negative control lenses (Figure 3-8.B). These peaks are likely due to the laser interacting with the inherently reflective surface plasma coating of lotrafilcon B.[15, 151]

CE-NBD was imaged using CSLM, which is a useful tool that allowed for analysis of

deposition at different depths of the CL. However, it is not ideal for data collection that requires the accommodation of a wide range of fluorescence intensities. As seen with this study, different gain settings and scaling factors were used to encompass both the low RIF at day 1 and high RIF at day 30. In addition, the quantum yield of the fluorophore may differ depending on the lens material. For this reason, using the RIF values to correlate the relative amount of deposition between different lens materials could not be compared.

3.5 Conclusion

CE-NBD deposited in all four lens types tested. Regardless of lens type, the amount of lipid deposition increased over time. This accumulation of lipid over time may play a role in perceived comfort experienced during CL wear. Practitioners should consider the effect of accumulated CL deposition on a patient-specific basis when recommending daily wear modalities. Two silicone hydrogels, senofilcon C and comfilcon A, exhibited uniform CE-NBD deposition whereas the other two silicone hydrogels, lotrafilcon B and samfilcon A, exhibited more lipid deposition on the surfaces. Different deposition profiles of lipid may have varying effects on the ocular surface, such that surface deposits on the CL interact more readily with the surrounding tear film, versus a limited interaction of lipids sequestered within the bulk of the lens.[82, 106, 108] Overall, the accumulation and location of CE-NBD deposition varied depending on the lens material. Future work is needed to determine whether the effect of surface and bulk lipid deposition on the CL is deleterious. A better understanding of how lipids interact with CL may provide new insights on improving lens materials to meet the increasing demand for more comfortable CL wear.

To simulate CL wear, a simple vial model was used in this study. However, this type of model lacks several physiological interactions between the CL and the ocular environment. To study CL deposition in a more clinically relevant setting, an *in vitro* eye model (OcuFlow) was developed at the

CCLR. OcuFlow consists of a synthetic eye and eyelid pieces, which are mounted onto a platform that can be integrated with any commercial microfluidic system to provide controlled tear flow. In addition, movements of the eye and eyelid piece allow for simulated intermittent air exposure and friction experienced during blinking. While this model received considerable positive feedback from the field, it still lacks several key elements that need to be addressed. Two additional factors that are important to better simulate on-eye conditions are the vertical blink mechanism and a layered tear film structure. The next two chapters will discuss the advancements made to overcome these two challenges in OcuFlow II.

Chapter 4 – Designing A Blink Mechanism in an *In Vitro* Eye Model

4.1 Introduction

As the expanding CL field continues to introduce new advancements and technologies, there is also an increase in demand for better testing methods of these new lens materials. Currently, options for testing different CL parameters and their interactions with the eye are somewhat limited. For example, the majority of *in vitro* CL studies[60, 64, 100-105] are performed using static vial methodology, as described in the previous chapter, which greatly exceeds physiological tear amounts of 6.2 µL,[21] in addition to lacking tear flow and a blink mechanism. To address this, our lab developed the OcuFlow I (Figure 4-1),[113] which is an *in vitro* eye model that simulates the human eye and allows for CL testing with relevant on-eye parameters.

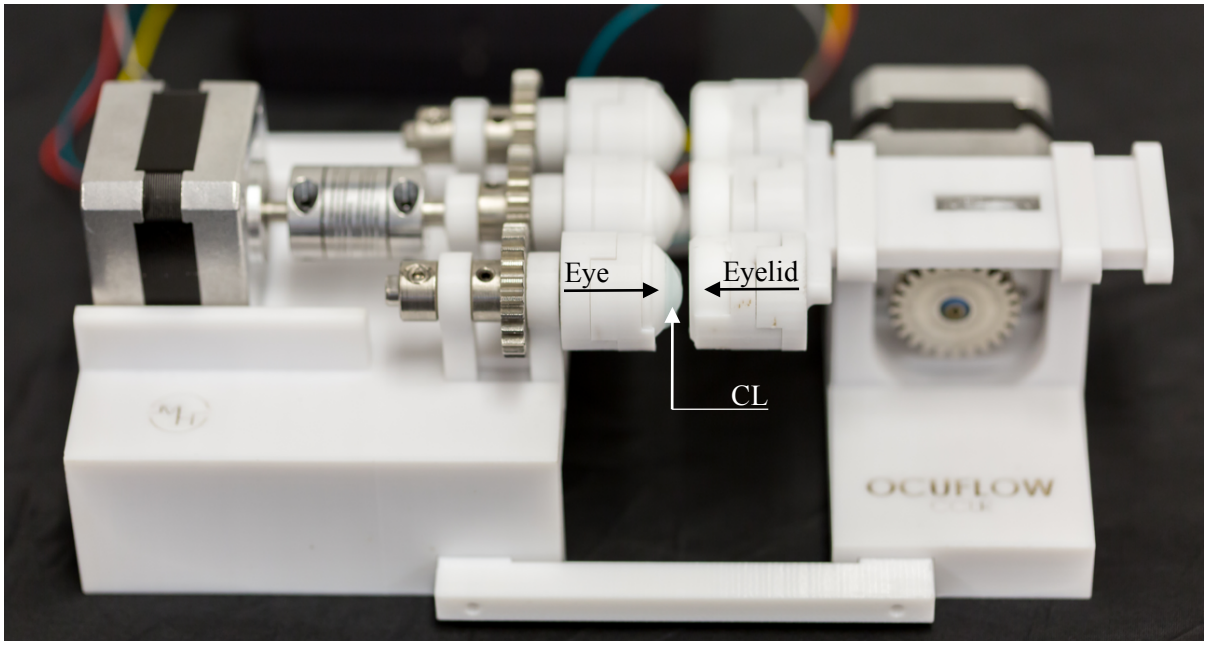

Figure 4-1. Photograph of the OcuFlow I model

The initial iteration of the blink mechanism on the OcuFlow I (Figure 4-1) was designed with

simplicity in mind, to allow for efficient prototyping. The blink motion was broken down to two fundamental movements; a rotational movement of the eye piece and a lateral movement of the eyelid piece. However, rather than a rotational and lateral motion, a natural blink or lid saccade is a combination of rotational and vertical motion.[152] The lack of accurate motions prevented representative forces from being applied onto the CL and surrounding tear solutions, which have a significant impact on the CL as well as the cornea.[153]

Blinking is a semi-autonomic response that serves to provide lubrication and protection of the anterior surface of the eye as well as visual information processing.[154] The blink mechanism consists of two phases, the opening and closing phase, which involves several muscles around the eye to move the eyelid. The opening phase is maintained by the contraction of the levator palpebrae superioris muscle and relaxation of the orbicularis oculi.[152] Vice versa, the closing phase is driven by the contraction of the orbicularis oculi and relaxation of the levator muscle. The OcuFlow II eye model was designed with these muscles in mind. This chapter will discuss the development and progressive advancements made in introducing a tangential movement to the eyelid in order to simulate a natural blink on OcuFlow II.

4.2 Iteration 1

One of the goals of the OcuFlow II project was to create an eye model with a mechanically representative blink motion. The design can be broken down into three main components: an eye piece, an eyelid piece and a platform to actuate the vertical blink mechanism. The blueprints for each component were first created using SolidWorks (Dassault Systèmes SOLIDWORKS Corp., Waltham, MA), a computer-aided design software, and then prototyped using 3D printing technologies.

4.2.1 Eye Piece

Ideally, the eye piece designed would mimic the human eye as much as possible, from its shape to its surface properties. The bulk of the eye piece is based on a semi-circular dome shape, representing the anterior surface of the eyeball (Figure 4-2).

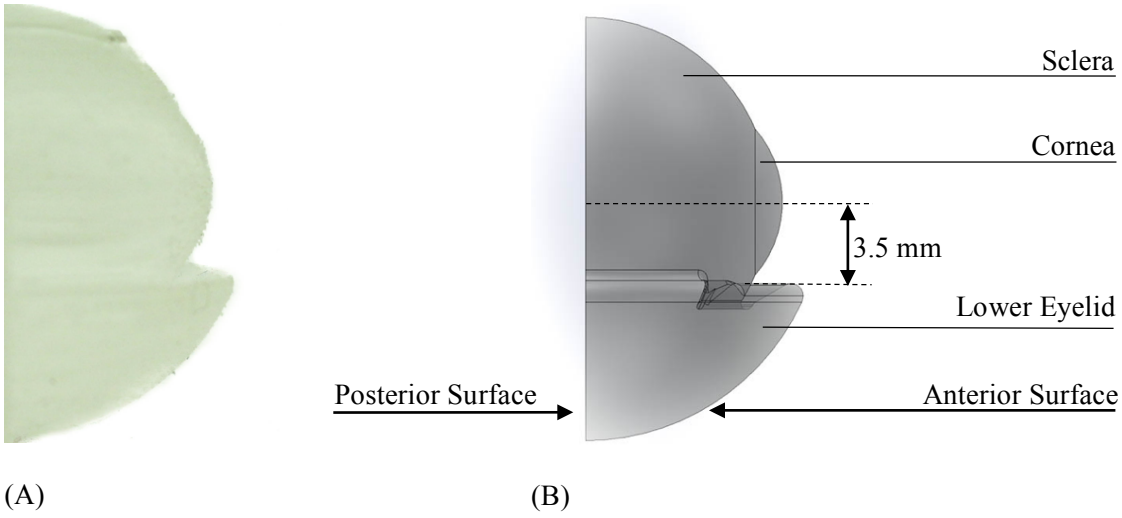

Figure 4-2. Side view of the synthetic PDMS eye piece (A) and computer model depiction (B).

The main portion of the eye piece (to represent the sclera) measures 24 mm in diameter, with the smaller dome (to represent the cornea) measuring a 14.5 mm in diameter, reflecting the average corneal shape on which a CL base curve would overlie. Along the bottom of the eyeball dome, a lower eyelid was designed as a fixed structure positioned 3.5mm below the center of the cornea with an outer diameter of 31 mm (Figure 4-2.B). Although the lower lid participates in a human blink, we decided its limited movement compared to the upper lid is insignificant[152, 155] and was designed as a fixed structure. The main functions of the lower eyelid on the model were to provide a cavity for tear collection as well as to prevent the CL from sliding off the cornea. In addition, the lower eyelid provided an eyelid margin for the upper eyelid to rest upon in order to achieve the closed phase of the blink.

Some important properties considered for the anterior corneal surface included a smooth texture, a spherical shape to effectively accommodate the placement of a CL, as well as relative inertness to enable testing with different compounds, including proteins, lipids, mucins and drugs with differing properties. With these criteria in mind, polydimethylsiloxane (PDMS) (184 Silicone Elastomer, Dow Corning, Midland, MI) was initially selected as the material to create the eye pieces. PDMS is an inert silicon-based organic polymer and is known for its suitable rheological properties,[156] which decreases the material's viscosity when heated and hardens when cooled. Taking advantage of this property, the eye pieces can be easily created by pouring heated liquid PDMS into a mold, which was then cured upon cooling. The mold was designed with the negative shape of the eye piece and the lower lid (Figure 4-3.A). Additive manufacturing was determined to be the main method of prototyping for this mold, due its cost effectiveness and rapid turnaround time. The first iteration of the mold was 3D printed using a fuse deposition modeling (FDM) method, which feeds thermoplastics into a heated nozzle to build models using the molten filaments. The thermoplastic material selected was acrylonitrile butadiene styrene (ABS) (University of Waterloo, Waterloo, ON), chosen for its ability to withstand high temperatures without deformation, which is a crucial step in the PDMS curing process. However, FDM technology is restricted by the size of the printer nozzle, which limits its precision and induces ridges on the surface finish of the PDMS mold (Figure 4-3.B).

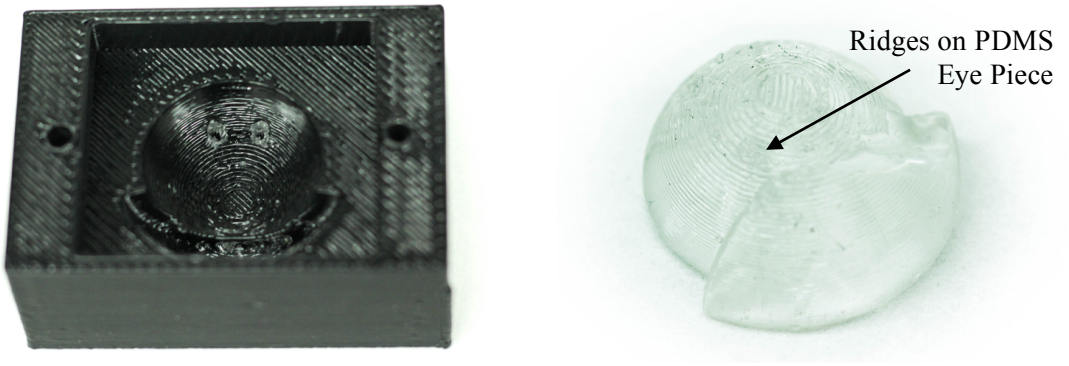

(A) ABS Mold (B) Complimentary PDMS eye piece

Figure 4-3. ABS mold (A) and its complimentary PDMS eye piece (B).

To achieve a smoother finish, an alternative resin-based printing technology, stereo lithography (SLA), was used. This method uses a computer guided ultraviolet laser to etch patterns in a pool of photosensitive liquid resin to create objects with a smooth surface finish. A polypropylene material, RGD450 (Hyphen – Christie Digital System Inc., Waterloo, ON), was used to achieve a glossy finish on the eye mold (Figure 4-4A). However, the resulting eyeball pieces were difficult to extract due to PDMS adhering onto the mold, causing pieces of the hardened PDMS to be left behind on the mold during extraction. Subsequently, a third type of printing technology called selective laser sintering (SLS) was used. SLS builds models in a pool of powder resin using laser curing methods similar to SLA. DuraForm PA (Hyphen – Christie Digital System Inc., Waterloo, ON) powder was selected to create a mold (Figure 4-4.B), which did not produce rough textures as observed from FDM and also avoided the glossy surface finish resulting from SLA. The uniform and matte surface finish of the mold from SLS allowed for easy extraction of the PDMS pieces (Figure 4-2.A) after curing. To ensure consistent depth between the eye pieces, a release channel was designed on the mold cap, which allowed excess PDMS to flow out of the mold when the mold cap was placed on (Figure 4-4). Although PDMS is the polymer selected for testing, the eye pieces can be created from any material,

ranging from various organic to inorganic polymers using the molds for increased research versatility.

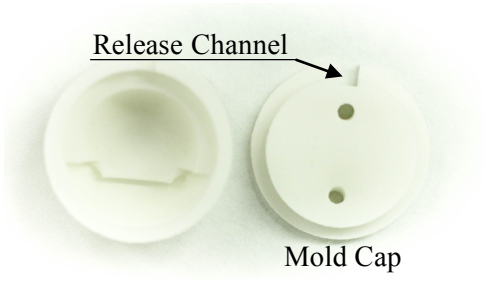

(A) Polypropylene Mold (B) DuraForm PA Mold

Figure 4-4. Eye molds printed from polypropylene (A) and DuraForm PA (B). The mold cap served to cover the mold to create a consistent eye piece.

4.2.2 Eyelid Piece

The human eyelid consists of a supporting tarsal plate and the skeletal orbicularis oculi muscle, which are lined by conjunctiva internally and skin externally. To mimic the eyelid, the model eyelid piece must be flexible, durable, and chemically resistant. The initial method of constructing the eyelid pieces followed closely with the 3D manufacturing steps introduced in the previous section using molding techniques (Figure 4-5). As the counterpart to the eye piece, the eyelid piece (Figure 4-5.D) is composed of a thin curved film section representing the lid and a thick flat region representing the lid margin. The film section is 0.5 mm thick with a spherical surface measuring at an offset of 250 μm from the outer edge of the eye piece to account for the thickness of the CL. The lid margin, located along the bottom edge, has a thickness of 3.75 mm to provide three functions: to allow for contact with the lower lid margin, to allow for the application of an upward force by the motor and to allow for the implementation of fluid ducts to enable tear flow.

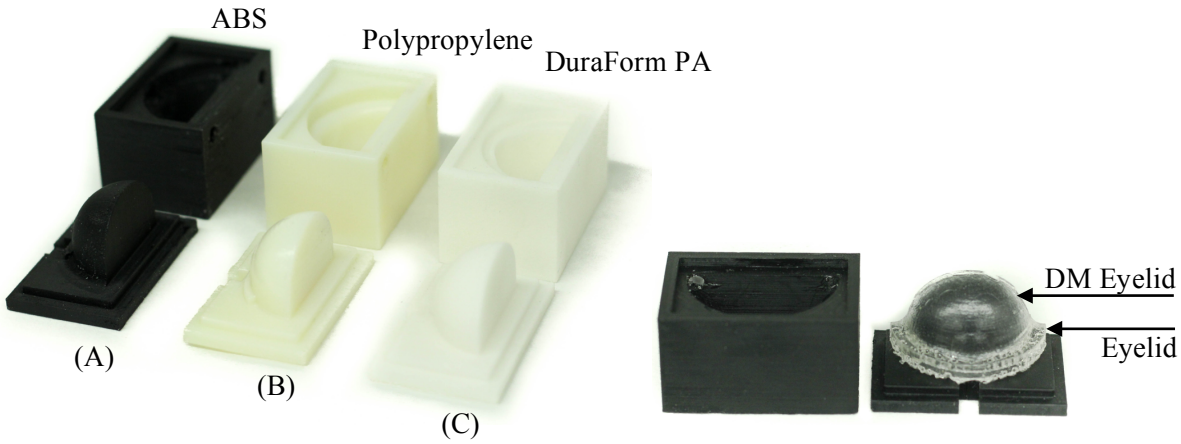

Figure 4-5. Eyelid molds constructed from ABS filaments (A), polypropylene (B), and DuraForm PA (C).

However, due to the added complexity of being thin and flexible, the resulting PDMS eyelids were too fragile and could not withstand repeated testing. Hence, a different resin material, Digital Materials (DM) (Hyphen – Christie Digital System Inc., Waterloo, ON) was selected to laser print the eyelid shape directly. DM98 is a series of materials composed of assembled voxels that have rubber like properties with a range of softness.[157] With the thin film structure in mind, DM9855 was chosen for the best balance between Shore hardness (stiffness), tear resistance (mechanical durability) and tensile strength (flexibility).

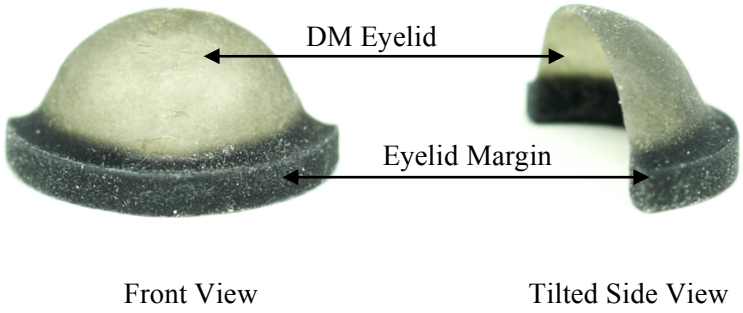

Figure 4-6. DM eyelid piece OcuFlow II iteration 1 platform 1.

4.2.3 Mechanical Platform & Setup

The platform brings integrity to OcuFlow II by providing a mechanism to install the model eye in an upright position as well as housing actuating motors. Several iterations of the platform were designed and created to optimize its fit and function. Three different design stages will be described and explained in a sequential order, starting with platform 1.

Platform 1

Two key features were implemented in Platform 1, a clamp mechanism and a motor stage. The clamp mechanism was achieved by designing a spherical indented base (Figure 4-7.B) to hold the model eye and an adjustable horizontal plate to clasp the model eye in place using elastic bands (Figure 4-7.C). The model eye consisted of an eye piece and eyelid piece attached along the upper margin with permanent adhesive (Figure 4-7.A). In addition, the corners of the eyelid pieces were connected to the eye piece by an elastic latex (Figure 4-7.A), leaving the lid margin with freedom of movement.

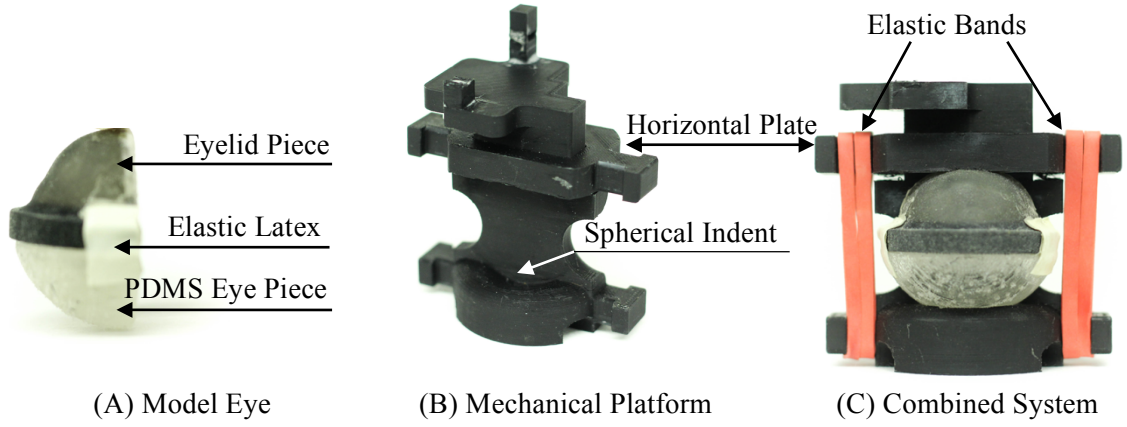

Figure 4-7. OcuFlow II iteration 1 platform 1 photograph depicting the clamping mechanism.

The second feature was the stage (Figure 4-8), constructed at the top of the platform to provide a space for the motor. A compact servo motor (SG90) (RobotShop Inc., Mirabel, QC) was selected

and used to automate the blink motion. This type of motor contains a feedback mechanism that allowed for precise angular positioning along the motor arm, which was crucial for controlling the repeated opening and closing positions of the eyelid accurately. By connecting the motor to the top part of the eyelid margin via a monofilament (nylon 275YD) cord (McMaster-Carr, Elmhurst, IL) (Figure 4-8), the eyelid piece was pulled open with the tension exerted onto the cord, simulating the open phase of a blink through the contraction of the levator muscle on the eye. A cord was used rather than a solid rod, because a cord better mimics the mechanism of muscle contraction in the eye. A force was only applied when the levator contracts to open the lid, while no force was applied when the levator relaxes when the lid closes. During the closing phase, the tension in the cord relaxed as the motor rotated in the opposite direction and the eyelid returned to its original position from the natural retraction of the two elastic latex, simulating the contraction of the orbicularis oculi. After repeated testing, it became clear that the point force applied to the flexible eyelid margin using the nylon cord did not provide consistent force along the whole eyelid, resulting in tears at points of repeated folding. In addition, a significant amount of frictional force experienced between the eye and eyelid piece was not accounted for by the SG90 servo motor and was determined to have inadequate torque to sustain repeated movements.

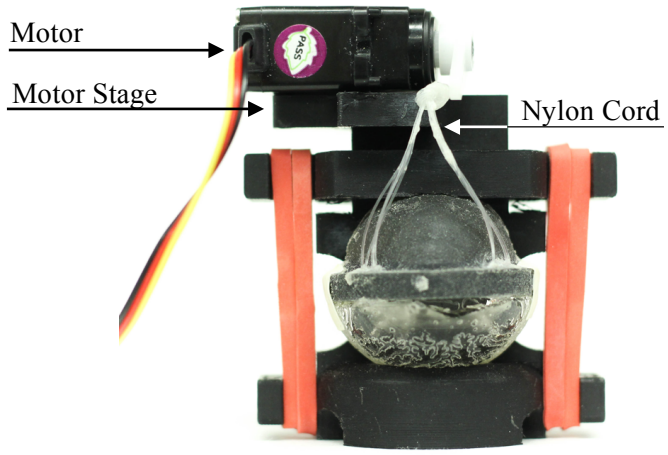

Figure 4-8. OcuFlow II iteration 1 platform 1 photograph depicting the motor and the associated blink mechanism.

Platform 2

In platform 2, the way in which the eyelid piece interacts with the eye piece was changed, to provide a mechanism that allows for even distribution of force applied along the eyelid margin. In addition, a different eyelid piece made from polyvinyl alcohol (PVA) (Sigma-Aldrich, St.Louis, MO) was introduced to the setup (Figure 4-9.A). PVA enabled the design of an extremely thin, flexible, and hydrophilic eyelid piece. Its smooth surface also significantly reduced the frictional forces between the DM (eyelid) and PDMS (eyeball) materials observed previously in platform 1. To allow for movement of the PVA eyelids, it needed to be secured to a rigid edge on the eyelid piece. Adding onto the original platform, a separate eyelid ledge piece was printed out of ABS (University of Waterloo, Waterloo, ON) to create a solid eyelid margin (Figure 4-9.B). The new eyelid piece consisted of a semi-circular ring that rotates along two pivots over the corneal eye piece. At the centre of the eyelid ledge was a loop allowing for easy attachment of the nylon cord stemming from the motor. The eyelid ledge was seated over a flat base and could easily slide into the modified base of the main platform. The PDMS eye piece was placed behind the eyelid ledge, which was attached to

the PVA eyelid along the margin (Figure 4-9.C).

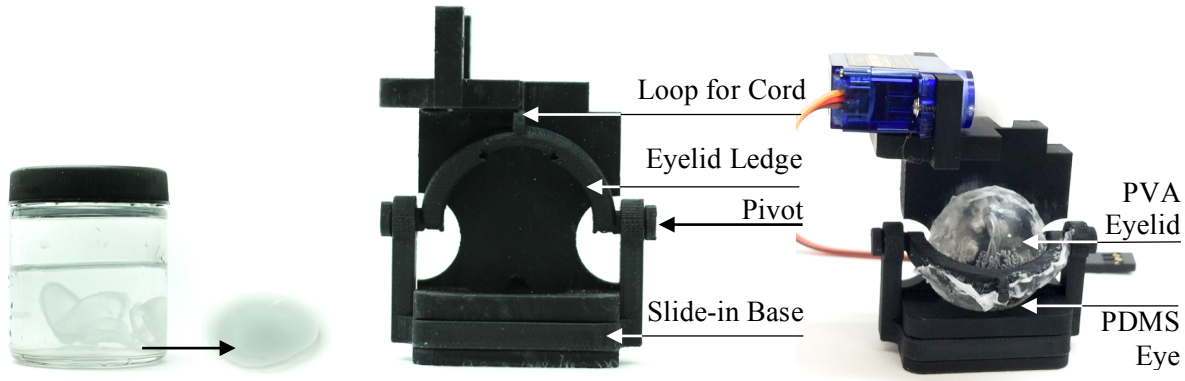

(A) PVA Eyelid (B) Mechanical Platform (C) Assembled Platform

Figure 4-9. OcuFlow II iteration 1 platform 2 setup.

Platform 2 was designed with the main goal of testing the functionality of the eyelid ledge piece, in addition to the interaction between the PVA eyelid with the rest of the platform. The rigid eyelid ledge proved to withstand repeated testing and provided more reliable movements. However, due to PVA's nature of deforming when it is not hydrated,[158] it was difficult to maintain a consistent eyelid shape. This prevented repeatable and controlled observations of the CL and its interaction with the platform and hence this design was determined to be inadequate.

Platform 3

The goal of platform 3 (Figure 4-10) was to create a functional unit based on learnings from platforms 1 and 2.

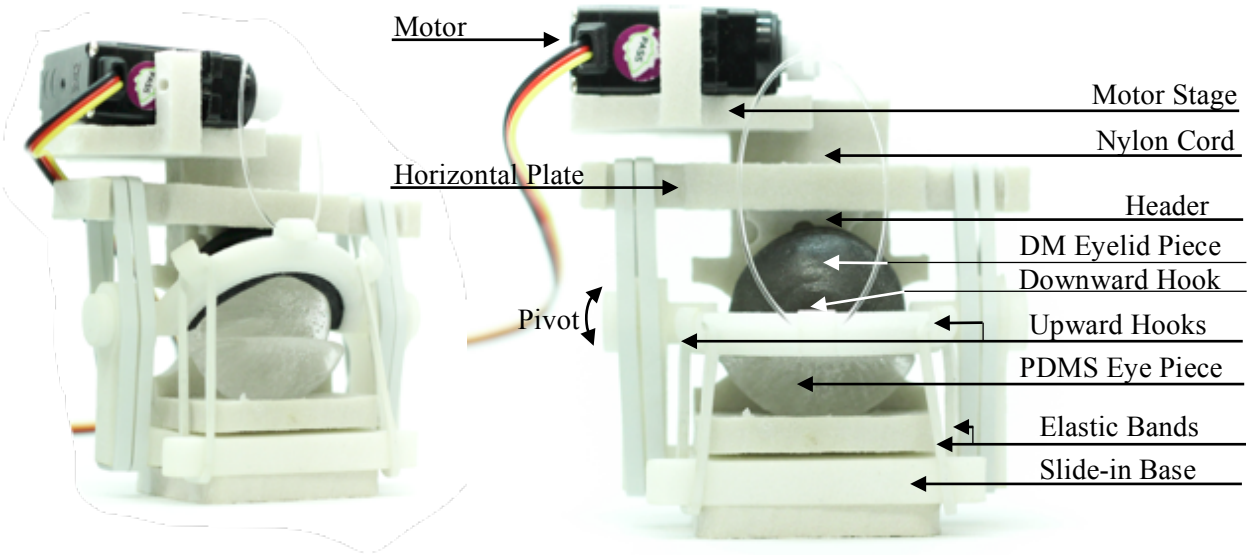

(A) Opened Phase (B) Closed Phase

Figure 4-10. OcuFlow II iteration 1 platform 3 photo depicting the opened (A) and closed (B) phase of the blink.

Firstly, the horizontal plate was modified with a header at the front to better clamp the eyeball piece in position. Secondly, a groove was added along the eyelid ledge to allow the attachment of the DM eyelid margin, which was modified to fit the groove accordingly. Applying force on the rigid eyelid ledge instead of the flexible eyelid allowed the force to be evenly distributed during the opening and closing phases of the eyelid. Thirdly, a downward facing hook was implemented at the centre of the rigid eyelid ring to provide an anchor for the nylon cord to connect to the motor arm. Fourthly, two upward facing hooks at each side of the eyelid ledge were installed to connect to the base through two elastic bands, replacing the glued latex bands between the eyelid and eye piece from platform 1. The elastic bands served to provide a downward force required during the closing phase of the lid, when the nylon cord relaxes. Lastly, a different servo motor (HS-85BB) with stronger torque was selected for its ability to withstand repeated testing while maintaining a compact size

(Figure 4-11). The electronic component of the OcuFlow II setup consisted of a motor, an Arduino board, and a power source. The motor was connected to an Arduino board, which acts as the main controller. The speed and position of the motor can be programmed by connecting the Arduino board to any computer as the power source.

One concern of platform 3 was to ensure proper spacing between the movable components. In particular, the horizontal plate must be printed in an interlocked state with the main platform and the two pivots on the eyelid ledge must be printed with accurate spacing to allow for a functional axle. To prevent obstructed movements and slanting between the movable parts, iterative printing methodology was used to achieve optimal spacing between those two crucial mechanisms.

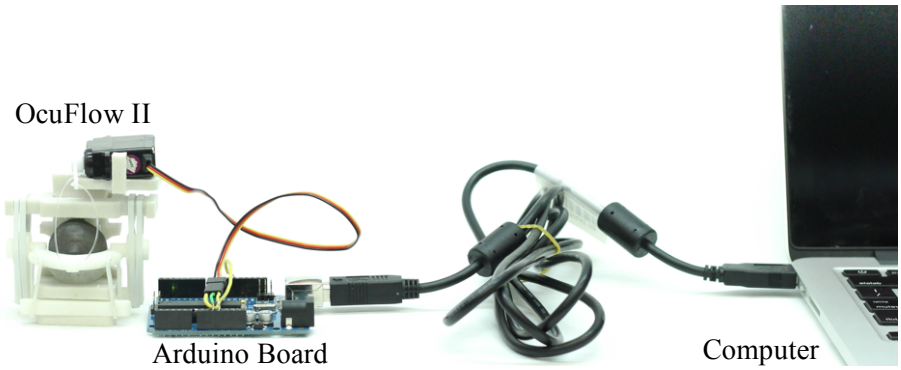

Figure 4-11. OcuFlow II iteration 1 platform 3 electronic component setup.

The first two platforms were 3D printed from ABS (University of Waterloo, Waterloo, ON), which is cost effective to produce and allows for fast turnaround time. However, the porous natural of the material resulted in unwanted absorption of solutions during testing. With this limitation in mind, the following two iterations were created using DuraForm PA (Hyphen – Christie Digital System Inc., Waterloo, ON), which can be made from a blend of different resins to achieve its waterproof property to enhance biocompatibility.

Limitations

In this setup, we attempted to create a comprehensive blink setup with an eye piece, a pliable yet durable eyelid piece, a functional platform, a robust motor and a controller with flexible programming capabilities. After testing platform 3, the two limitations that remained were the insufficient spacing for the eyelid piece to fold during the opening phase of the blink and the inconsistent force provided by the nylon cord and elastic latex. When the eyelid is pulled back to an open phase, the eyelid folds against the platform pillar, which can come in contact with the CL placed on the eye piece and result in tears after repeated testing. Moreover, the applications of the nylon cord and elastic band using to open and close the eyelid introduced inconsistency in the amount of force applied to the system. Specifically, the elastic band can change the force applied drastically over use. As a proof of concept, these materials were more than sufficient, but for reliable and repeatable results, materials with tighter tolerances and long term reliability testing are required. Unfortunately, these limitations require fundamental changes to the setup, which required a significant amount of redesign. From this design process, we learned that trying to implement too many features at the same time is not practical. The inconsistent and tedious nature of the setup required a fresh start to create a simpler and more reliable platform.

4.3 Iteration 2

The main goal of iteration 2 was to create an eye model with a vertical blink that also allowed for easy and consistent assembly. To achieve this, the OcuFlow II setup along with the eye piece, eyelid piece, and platform were redesigned.

4.3.1 Eye Piece

Adopted from iteration 1, the eye pieces in iteration 2 had the same general dome structure with

a fixed lower lid. Initially, the lower lids were created out of PDMS using molds. However, PDMS is hydrophobic and does not reflect the surface of the human cornea. To explore different options, the eye pieces were 3D printed using a white nylon (PA 2200) material (Think2Thing Inc., Toronto, ON), which is more hydrophilic, as demonstrated by the greater contact angle of ~72° using the sessile drop technique (Figure 4-12).

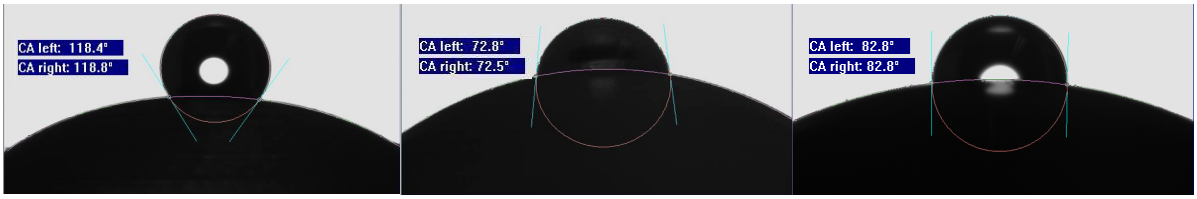

(A) PDMS (B) Nylon (C) Acetal

Figure 4-12. Advancing water contact angles of PDMS (A), Teflon (B), and Acetal (C) eye piece surfaces measured using sessile drop technique.

During testing, the rough unpolished surface of the nylon eye piece proved to be problematic and introduced too much spacing and air bubbles between the CL and corneal surface. In addition, the white colour of the eye piece was too reflective and prevented subsequent testing using several clinical instruments, which are designed and calibrated for the coloured human iris. To overcome these limitations, the eyelid pieces were machined out of polyoxymethylene polymer, also known as acetal (University of Waterloo, Waterloo, ON), which is more hydrophilic than PDMS (Figure 4-12) and is inherently black in colour (Figure 4-13.D). Two holes were drilled along the posterior surface of the eye pieces to allow for attachment to the platform (Figure 4-13). Due to its complimented structure, the lower eyelid was 3D printed separately using nylon (Think2Thing Inc., Toronto, ON) and attached to the eye piece (Figure 4-13.D).

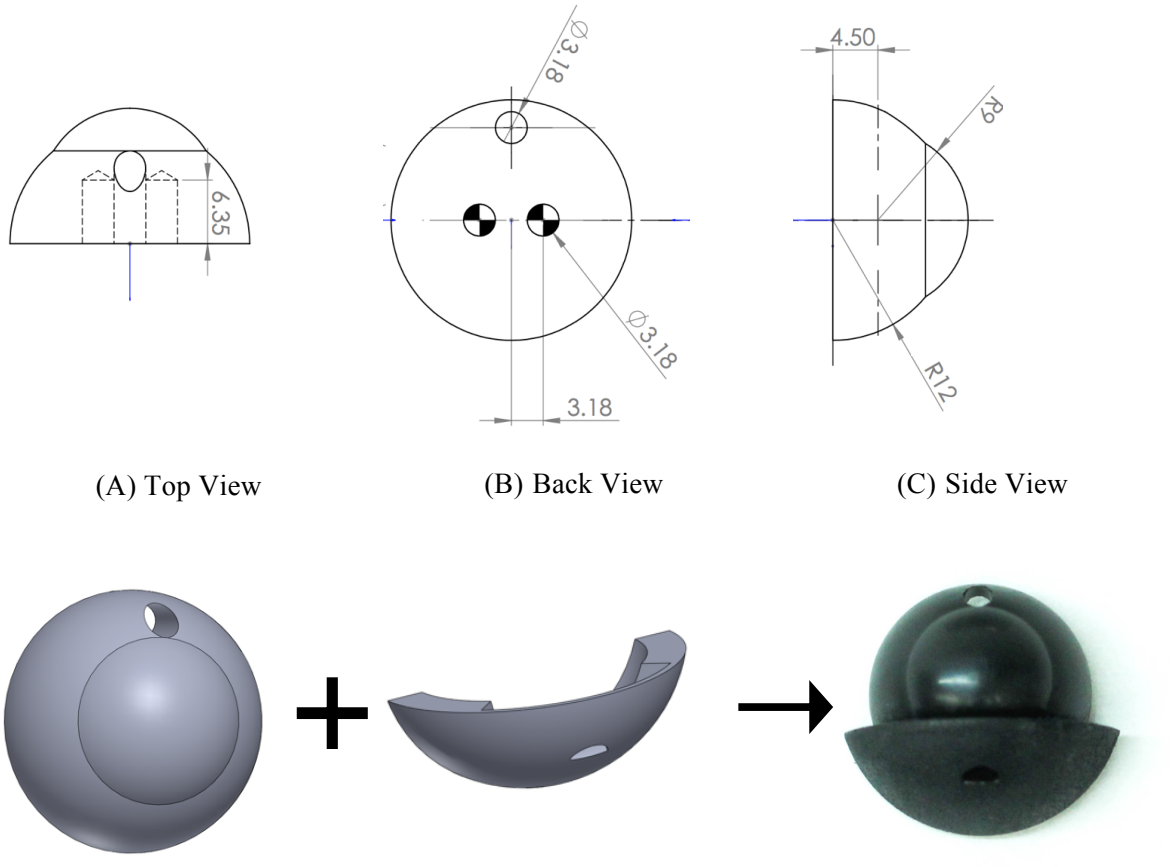

(A) Top View (B) Back View (C) Side View

(D) Assembled View

Figure 4-13. OcuFlow II iteration 2 eye piece with dimensions (A-C) and with the assembled lower eyelid (D).

4.3.2 Eyelid Piece

Instead of a flexible eyelid, a rigid eyelid was designed and 3D printed using nylon (PA 2200) (Think2Thing Inc., Toronto, ON). The eyelid piece (Figure 4-14) was composed of a concave eyelid component supported by an L-shaped bracket. The rationale behind switching to a rigid eyelid from a flexible one was to allow for consistency, increased structural integrity and efficiency in setup. The assumption made was that the eyelid served its function as long as the lid margin glides over the eye piece and is able to replenish the tear film.

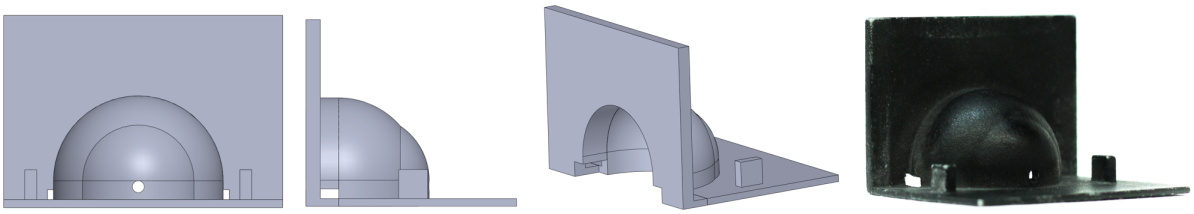

(A) Front View (B) Side View (C) Tilted Back View (D) Actual Photo

Figure 4-14. OcuFlow II iteration 2 eyelid piece.

4.3.3 Mechanical Platform & Setup

The platform in iteration 2 was easy to assemble and consisted of several different metal components held together by stainless steel rods (McMaster-Carr, Elmhurst, IL). The nine metal pieces (parts A-I) make up the body of the platform and are machined out of aluminum (University of Waterloo, Waterloo, ON) for good structural durability (Figure 4-15).

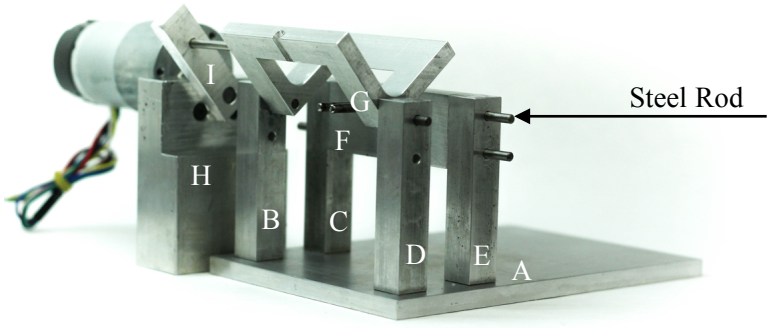

Figure 4-15. Aluminum assembly of OcuFlow II iteration 2.

Part A is a flat rectangular base to which other supporting structures are attached to. Parts B to E are identical pillars that are secured to part A and act as the support structures. The pillars allow for the attachment of parts F and G, which are responsible for affixing the eye and eyelid piece respectively. Part F is a rectangular block that is secured between the two back pillars using two steel rods on each side. In addition, two steel rods are press-fitted onto the front surface of part F to allow

for attachment of the eye piece (Figure 4-16.A). Part G is an L-shaped bracket that allows the complimentary eyelid piece to be easily clipped on (Figure 4-16.B).

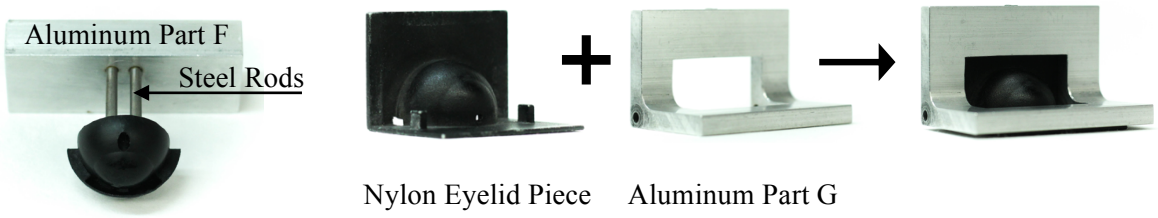

(A) Assembled Eye Piece (B) Assembled Eyelid Piece

Figure 4-16. OcuFlow II iteration 2 assembled eye piece (A) and eyelid piece (B).

The bracket is attached between the two front pillars with one steel rod at each pivot, which allows the eyelid to rotate via a motor. The motor is connected to the setup using part H and I (Figure 4-15). Part H is attached to the base (part A) with two press-fitted steel rods and serves to raise the motor so it is leveled with the eyelid piece. To move the eyelid, part I is installed to pivot along the motor and is connected to the aluminum bracket using a steel rod. A metal gear motor (100:1 with 64 CPR encoder, McMaster-Carr, Elmhurst, IL) is used to supply the torque need for to rotate the eyelid piece (Figure 4-17). Part H is attached to the base (part A) with two press-fitted steel rods and serves to raise the motor so it is leveled with the eyelid piece. The motor is connected to a micro Roboclaw controller (Pololu Corporation, Las Vegas, NV), which can supply up to three times the power output than an Arduino board when connected to an external DC power supply (Pololu Corporation, Las Vegas, NV) (Figure 4-17).

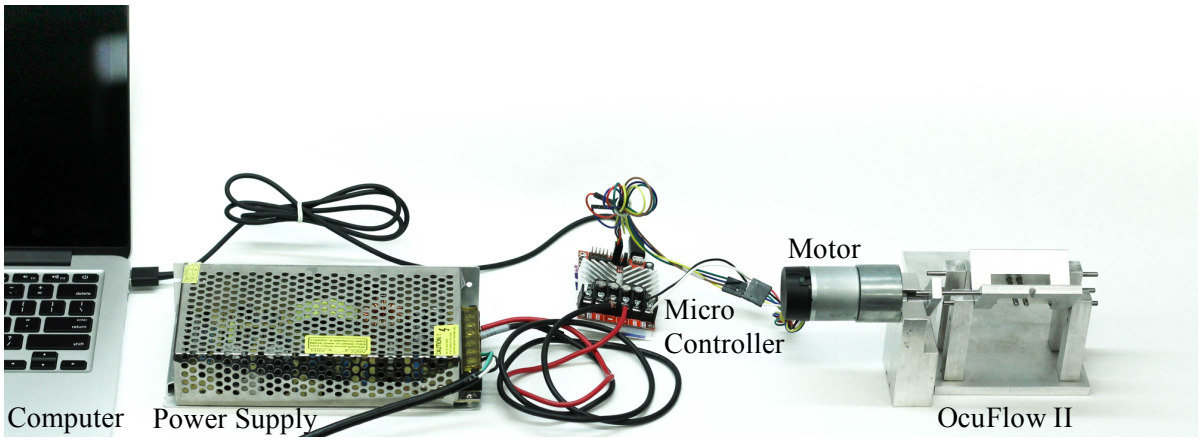

Figure 4-17. OcuFlow II iteration 2 setup.

By connecting the micro controller to the computer, the motor speed and position can be manipulated to account for the highly variable human blink rate, which averages around 14-17 blinks per minute[159, 160] for an interval of 2-10 seconds. The open position (Figure 4-18.A) is angled at 65° to the horizontal and is set as the start position to allow for insertion of a CL. When the motor rotates 65° downwards, the eyelid comes to a closed position in 0.3 sec (Figure 4-18.B). When the motor rotates 65° upward, the eyelid returns to an open position in 0.3 sec and maintains this position for 5.4 sec before the next blink, to simulate intermittent air exposure of the lens.

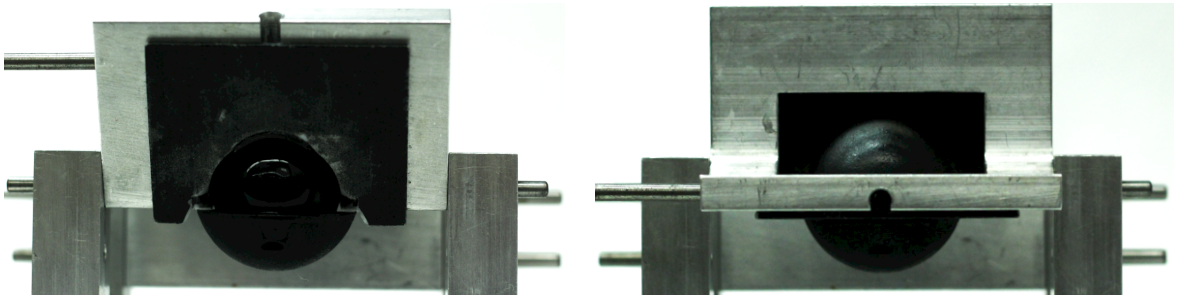

(A) Open Position (B) Close Position

Figure 4-18. Photo of eye and eyelid piece on OcuFlow II iteration 2 depicting the open and close position.

4.4 Conclusion

Traditional eye models lack a blink mechanism, which is an essential component of the ocular environment. The development of a novel *in vitro* eye model, OcuFlow II, with a sophisticated blink mechanism was described in this chapter. Developing a novel eye model is a highly iterative process that combines vision science and engineering. OcuFlow II evolved through several platforms before a functional model was made. The first iteration served as a proof of concept and attempted to mimic several aspects of the blink, including a semi-spherical eye, a flexible eyelid and representative muscle forces of the blink reflex. However, simulating too many features simultaneously resulted in several limitations to the model that require fundamental changes to the setup. Building on learnings from iteration one, a second iteration was designed with a much simpler setup to allow for consistent and reliable testing results. Iteration 2 also consists of an eye piece, an eyelid piece and a mechanical platform. Each component was designed to allow for an easy setup of a vertical blink mechanism between the eye and eyelid pieces. The design of iteration 2 is robust and proved to be successful in simulating a natural blink. CL can be tested with on-eye parameters by placing the lens onto the corneal surface of the eye piece. The mechanic blink allows testing of different lens material with more representative results. In addition, the developed blink mechanism allows for tear film formation on the corneal surface, which is another crucial component of the ocular environment and will be discussed in the next chapter.

Chapter 5 – Incorporation of a Tear Film into an *In Vitro* Eye Model

5.1 Introduction

Currently, the majority of *in vitro* CL studies are performed by immersing the lens in a vial containing 1 to 5mL of ATS,[60, 64, 100-105] which greatly exceeds the physiological tear volume of 6.2 µL.[21] In particular, these studies do not account for the impact of a representative tear film on the CL. The structure, stability and function of the tear film is greatly influenced by the blink mechanism.[161] OcuFlow I is an *in vitro* eye model with a blink mechanism that supports a tear film. As mentioned in the previous chapter, the rotational and lateral movements of the eye and eyelid piece in OcuFlow I is not reflective of a natural blink motion, which is a rapid downwards-upwards movement of the eyelid with a range of duration of approximately 0.1-0.4 sec.[152, 162-165] In OcuFlow I, the rotational motion of the eye piece against the eyelid piece introduces unnatural mixing of the different tear components. The lateral motion of the eyelid piece away from the eye piece breaks the surface tension and disrupts the integrity of the tear film. To overcome the limited movements in OcuFlow I, a more representative vertical blink was developed in OcuFlow II, to allow for a smooth regeneration and stable maintenance of the tear film. Moreover, OcuFlow I was designed with a single outlet on the eyelid piece to allow for controlled tear flow of a homogenous ATS.[113] However, the tear film consists of multiple phases rather than a homogeneous solution.[20, 22] Conventionally, the tear film consists of three distinct layers: the superficial lipid layer, the middle aqueous layer, and the innermost mucin layer. This somewhat simplistic view of the tear film has been challenged and a more recent understanding of the tear film is that it more closely resembles a bilayered structure, consisting of a distinct outermost lipid phase and a mixed aqueous/mucin phase with decreasing mucin concentration away from the cornea.[20, 23] To achieve a bilayered tear film structure, the lipid

and aqueous components must be secreted separately. The majority of the tear lipids are produced by the meibomian glands whereas the aqueous components are secreted from the lacrimal gland.[144, 166] A specific goal of OcuFlow II was to establish a system that allowed for the development of a bilayered tear film structure.

5.2 Iteration 1

In OcuFlow I, ATS was introduced into the system as a homogeneous phase through one outlet on the eyelid piece. The goal of OcuFlow II was to implement multiple outlets to allow for the delivery of distinctly separate tear components. As discussed in the previous chapter, iteration 1 evolved through three platforms. The next section will address these platforms with a focus on the tear delivery aspect of the design.

Platform 1

In platform 1, the eyelid piece was constructed by curing PDMS in a mold (Figure 5-1.A). Tear ducts along the eyelid margin were introduced by placing silicone tubes (VWR, Radnor, PA) into the designated opening on the mold (Figure 5-1.A) to simulate the meibomian glands. Upon curing, the PDMS eyelid hardened with the silicone tubes attached to both sides of the eyelid margin, where small openings were created to allow for delivery of tear solutions onto the eye piece (Figure 5-1.B). Silicone tubes, with an inner diameter of 0.063 inch and outer diameter of 0.125 inch, were selected for flexibility, durability, and inertness to different chemicals.

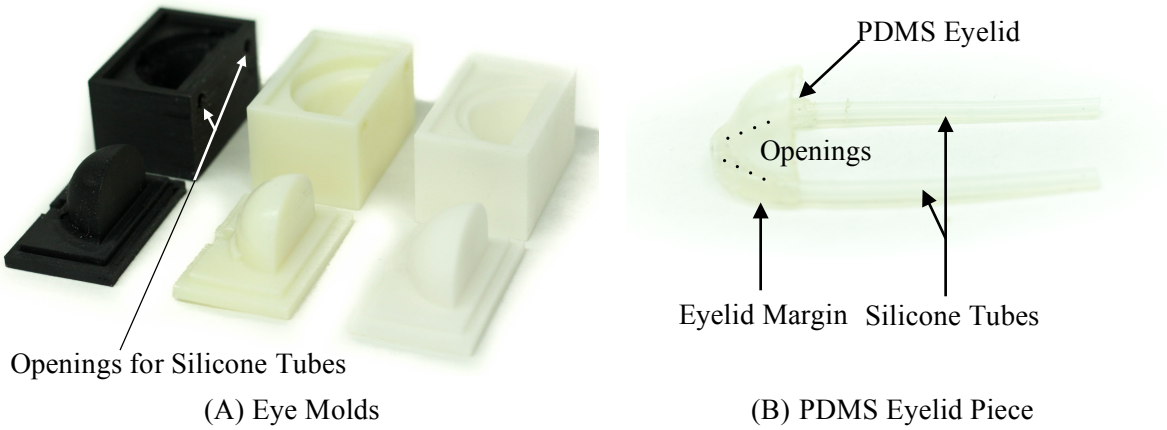

(A) Eye Molds (B) PDMS Eyelid Piece

Figure 5-1. Photo of the eyelid molds showing the opening for tubes (A) and PDMS eyelid piece with tubing on the eyelid margin (B).

However, the varying locations of the tear solution delivering openings resulted in inconsistent tear flow along the eyelid margin, where the openings further away from the source of the tear solution had significantly lower pressure and less tear flow. As mentioned in the previous chapter, PDMS eyelids were too fragile and brittle to withstand repeated testing. Hence, the eyelids were then 3D printed out of DM for enhanced durability (Figure 5-2). Unfortunately, the limited 3D printing technology did not allow ducts to be implemented on the constrained space along the eyelid margin.

Figure 5-2. DM eyelid piece of OcuFlow II iteration 1 platform 1.

Platform 2

In platform 2, an eyelid ledge piece was introduced, as seen in Figure 5-3. The eyelid ledge created space for the incorporation of pseudo-tear ducts along the rigid ledge. Rather than

incorporating several small openings along the entire eyelid ledge, only two openings were installed to avoid inconsistent pressure and flow. Tear flow was introduced to the system by inserting tubes into the two entrance openings on the eyelid ledge, which fed into two smaller exit openings at the front of the ledge (Figure 5-3.A). In addition to tear flow, a functional eyelid is a crucial component for generating a tear film to allow the spread of various tear film components over the ocular surface. PVA eyelids were implemented in platform 2 by attaching a thin film to the eyelid ledge. PVA was selected for its flexibility and was expected to glide smoothly over the corneal surface to create a tear film. However, PVA deforms as it becomes dehydrated and it is difficult to maintain a consistently hydrated state throughout the installation process onto the eyelid ledge.

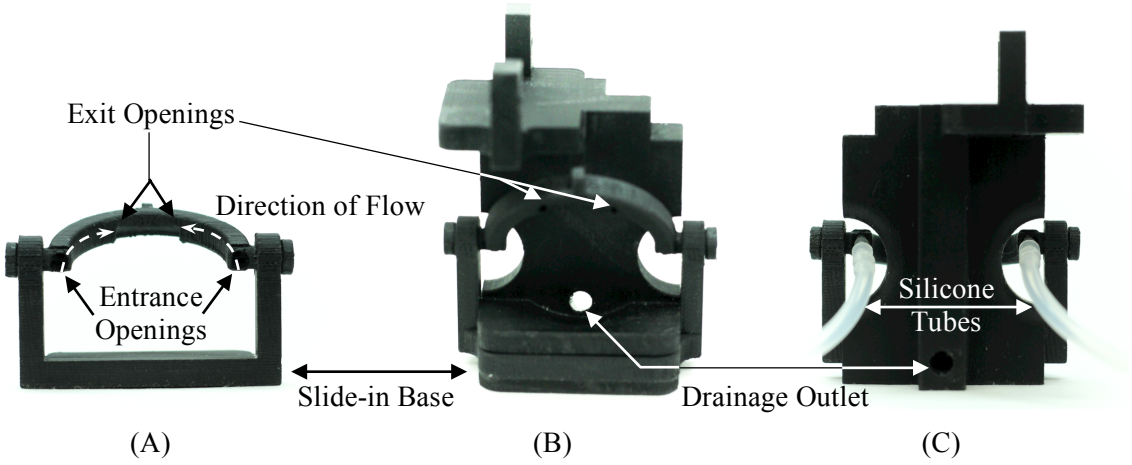

Figure 5-3. OcuFlow II iteration 1 platform 2 photo depicting the openings on the eyelid ledge piece (A) and the drainage outlet from the front view (B) and back view (C) of the mechanical platform.

Another feature implemented in platform 2 was the drainage outlet located at the bottom of the mechanical platform (Figure 5-3.B,C). The drainage outlet sits behind the eye piece and acts as the puncta. The drainage channel on the PDMS eye piece was created by temporarily placing a rod through the mold cap in place of the drainage channel upon pouring the heated PDMS into the eye

mold (Figure 5-4). Upon curing, the removal of the rod created the desired drainage route in the eye piece that connects with the drainage outlet on the platform.

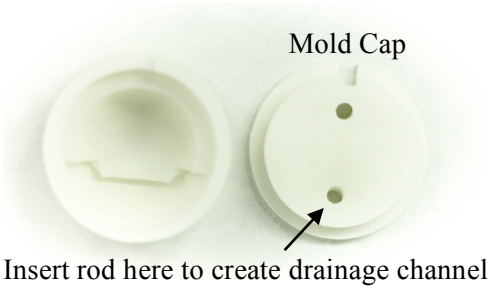

Figure 5-4. Eye mold depicting the opening of the drainage channel.

Platform 3

Similar to platform 2, two entrance openings were implemented on each side of the rigid ledge on platform 3, which fed centrally and anteriorly into the two exit openings (Figure 5-5.A). A groove was added to create spacing for the attachment of a flexible DM eyelid piece (Hyphen – Christie Digital System Inc., Waterloo, ON) (Figure 5-5.A). On the eyelid piece, a rectangular opening was designed adjacent to the exit openings on the eyelid ledge to allow for tear flow onto the eye piece (Figure 5-5.A). The tear duct setup along the eyelid was designed to mimic the meibomian glands for lipid secretion. To mimic the secretion of the aqueous phase, an additional outlet was implemented at the top of the platform (Figure 5-5.C). Similar to the drainage channel, the corresponding fluid channel on the PDMS eye piece can be created during the curing process by placing a rod in the respective opening in the mold (Figure 5-5.B). As fresh tear solution replenished the tear film, the old tears were collected through the drainage outlet (Figure 5-5.C).

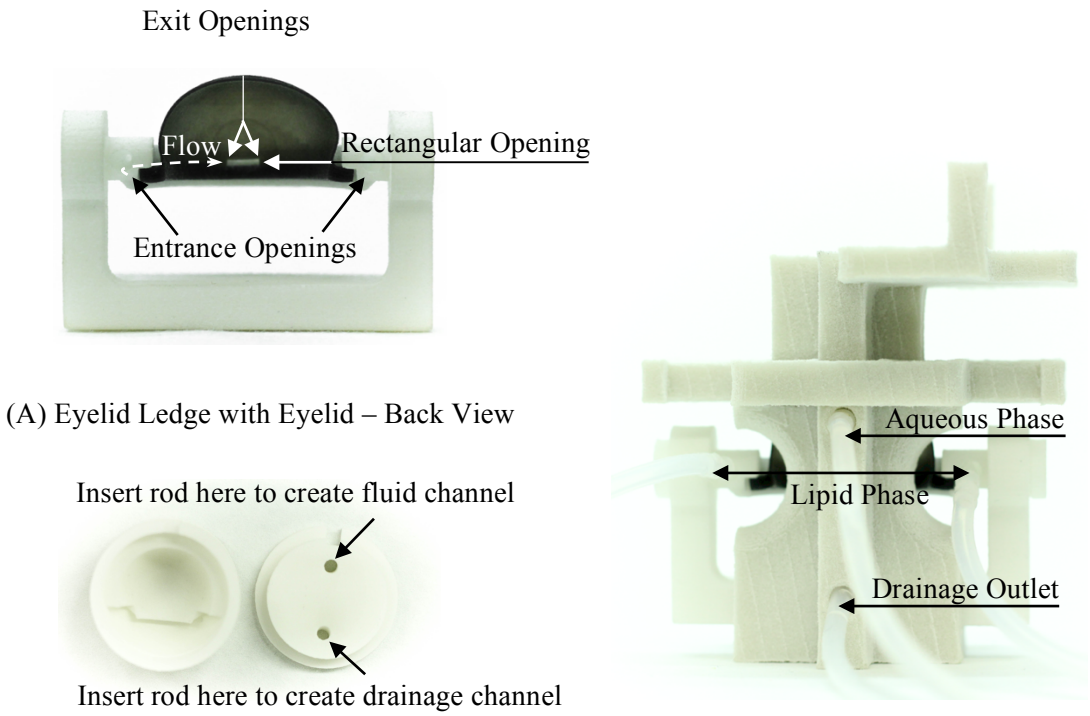

Figure 5-5. OcuFlow II iteration 1 platform 3 photo depicting the back view of eyelid ledge piece with an attached DM eyelid piece attached (A) and the back view of the mechanical platform with all the associated outlets.

Unfortunately, the blink mechanism in these platforms did not account for the proper folding of the eyelid piece during the upward blink, which resulted in deformation of the eyelid piece after repeated testing. As mentioned in the previous chapter, iteration 2 was created to simplify and overcome the limitations of iteration 1.

5.3 Iteration 2

The assumption made in designing iteration 2 is that a rigid eye and eyelid piece would provide reproducibility and repeatability. Hence, each component of the platform adopted a rigid design. In iteration 2, two fluid delivery sources were implemented on the eye and eyelid piece to allow for the

separate secretion of the aqueous and lipid phase respectively (Figure 5-6.A). On the eye piece, a through hole was designed centrally above the corneal surface (Figure 5-6.B) to simulate the lacrimal gland and allowed the delivery of the aqueous phase onto the eye model. On the eyelid piece, an opening was designed on the anterior corneal segment (Figure 5-6.C) to simulate the meibomian glands and allowed for delivery of the lipid phase onto the eye model. A circular groove was milled along the bottom ledge of part G to provide a channel for silicone tubes (Figure 5-6.D). Barbed tubing couplers (equal leg 1.6 mm diameter, VWR, Radnor, PA) were used to attach the silicone tubes to the outlets to ensure a secure connection that was able to endure the repeated blinking motion (Figure 5-6.A).

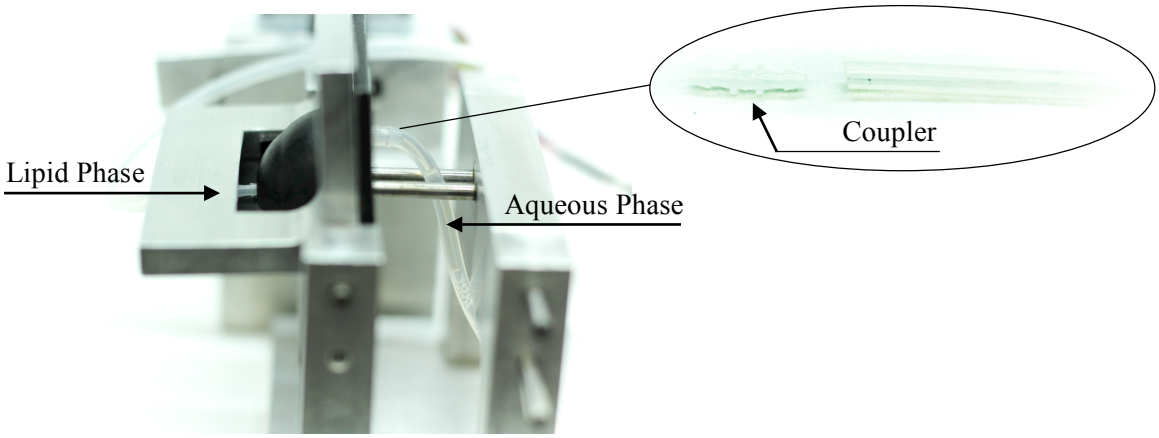

(A) Mechanical Platform – Side View

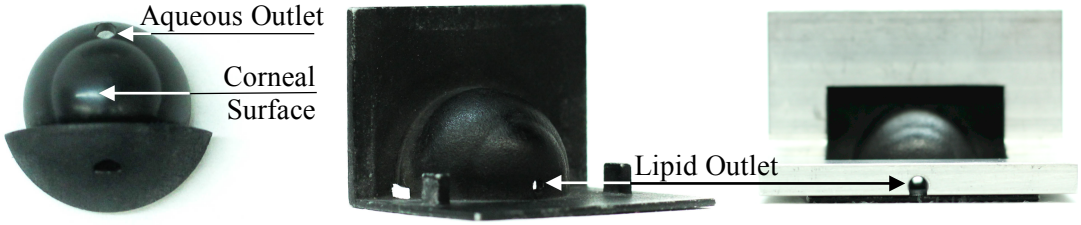

(B) Eye Piece (C) Eyelid Piece (D) Aluminum Part G

Figure 5-6. OcuFlow II iteration 2 photo depicting the outlet for the aqueous and lipid phase (A), the aqueous outlet on the eye piece (B), the lipid outlet on the eyelid piece (C, D).

For a controlled tear flow into the system, the silicone tubes were connected to a programmable microfluidic syringe pump (model PHD ULTRA™ 4400, Harvard Apparatus, Massachusetts, United States) (Figure 5-7). The lipid phase was introduced onto the eyelid piece to assist the formation of a superficial layer, whereas the aqueous phase was introduced on the eye piece to allow for a layer adjacent to the corneal surface.

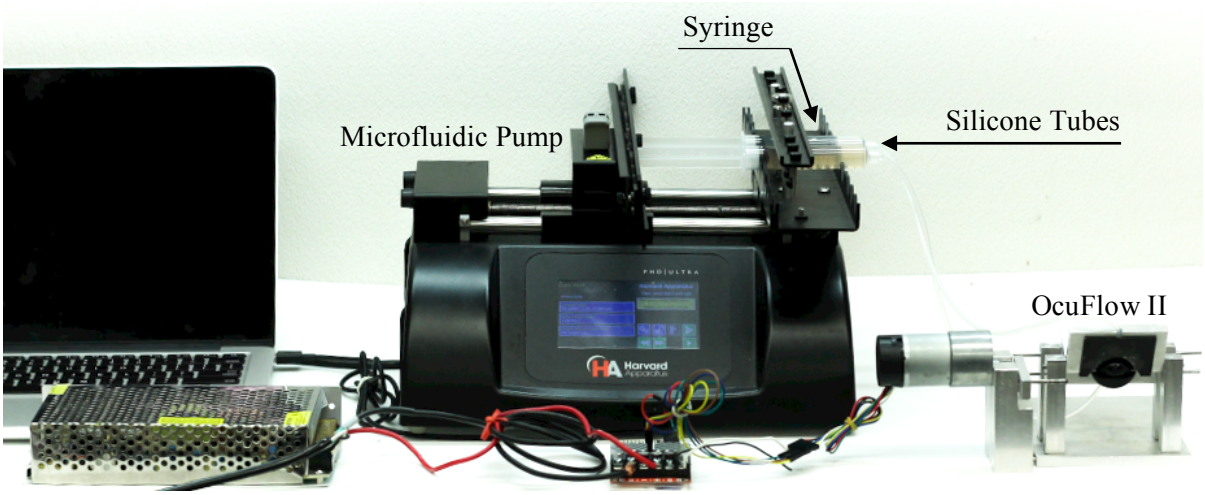

Figure 5-7. OcuFlow II iteration 2 setup depicting the microfluidic syringe pump.

In addition to tear flow, the blink motion must meet two criteria in order to generate the tear film. As the tear solutions gathered along the lower eyelid due to gravity, the upward blink replenishes the tear film, as the upper eyelid margin makes contact with the lower eyelid and spreads the pooled tear solution over the corneal surface. The first criterion is to allow the upper eyelid margin to make contact with the pooled tear solution along the lower eyelid. The second criterion is to allow the upper eyelid to glide smoothly over the corneal surface during the upward blink to maintain the spread of the tear film. However, it is difficult to follow the curvature of the eye piece, which is irregularly shaped, with a rigid eyelid. If the spacing between the eye and eyelid piece is too close, the eyelid will interfere with the eye piece and disturb the CL mounted on it. If the spacing is

too large, the surface tension of the tear solution will break between the eye and eyelid, resulting in a rupture of the tear film. To overcome this, a thin strip of flexible DM98 polymer (Hyphen – Christie Digital System Inc., Waterloo, ON) was adhered to the bottom of the upper eyelid piece (Figure 5-8.A) to create a more lenient eyelid margin, that allowed for a closer contact between the eye and eyelid piece without causing interference. This design enabled flexible spacing for the maintenance of a stable tear film. It is important that the ocular surface is replenished with fresh tears to remove debris and introduce nutrients to the anterior surface of the eye. To meet this demand, the eye is constantly secreting tear solution. As the old tears start to collect along the bottom eyelid, excess tears are transported to the puncta for drainage. To simulate this, an opening was designed on lower eyelid piece to allow for drainage of tear solutions (Figure 5-8.B).

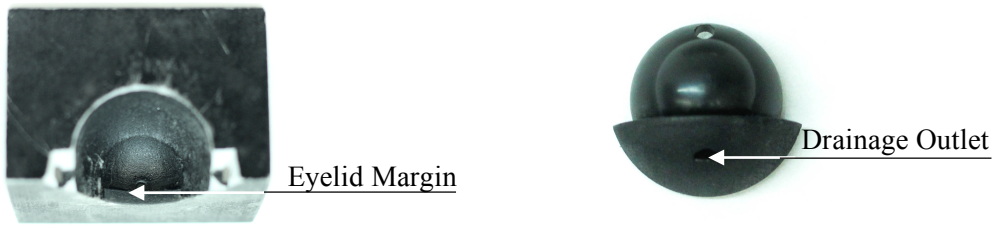

(A) Eyelid Piece (B) Eye Piece

Figure 5-8. Eyelid piece showing the DM eyelid margin (A) and eye piece showing the drainage outlet (B).

5.4 Conclusion

In OcuFlow II, a mechanism for tear film generation and replenishment onto the eye piece was established through an iterative process. In iteration 1, three platforms were described. In platform 1, tear ducts were implemented along the PDMS eyelid margin to simulate the meibomian gland. However, tear flow was not well controlled and varying amounts of tear solution were secreted, depending on the location of the opening along the eyelid margin. With the introduction of the rigid

eyelid ledge piece in the platform 2, two fluid channels were installed from either side of the ledge, which helped improve the control of the tear flow. An additional outlet was added to platform 2 on the eye piece to allow for separate delivery of the aqueous and lipid phases. Unfortunately, the PVA eyelid piece was difficult to handle and could not be reliably implemented into a functional unit. In platform 3, a functional eyelid piece was created by modifying the eyelid ledge piece to accommodate a SLS printed DM eyelid (Hyphen – Christie Digital System Inc., Waterloo, ON). Unfortunately, a stable tear film could not be maintained due to the erratic movement of the eyelid folding against the platform pillar, which interfered with the spread of tear solution during an upward blink. To overcome the limitations observed in iteration 1, iteration 2 was developed with a simpler setup. In iteration 2, the platform consisted of an aluminum assembly held together by stainless steel rods. Instead of a flexible eyelid piece, a rigid design was implemented to reduce variability during the blink movement. Similar to iteration 1, two sources of outlets were introduced in iteration 2 to allow for separate delivery of the aqueous and lipid phase, which were installed on the eye and eyelid piece respectively. Tear solution was introduced to the system by connecting the outlets to a microfluidic syringe pump via silicone tubes. The uniqueness of OcuFlow II was the implementation of additional outlets for separate delivery of the aqueous and lipid phase, which enabled the development of a layered tear film structure over the eye model. In addition, the blink mechanism introduced a changing ocular environment reflective of on-eye conditions and allowed for more representative testing of different CLs under physiologically relevant conditions. The easily modifiable components of OcuFlow II made it versatile in accommodating various study requirements. Although the fluid intake design was designed to simulate the glands in the human eye, any solution can be infused onto the system for a wide range of testing possibilities. Moreover, the eye and eyelid pieces can be modified and integrated with an animal cornea or eyelid, permitting more complex *in vitro* studies.

Chapter 6 – *In Vitro* Tear Break-up Time of Silicone Hydrogels Evaluated Using OcuFlow II

6.1 Introduction

The tear film is a vital component of a healthy eye and supplies nutrients, removes foreign particles, and acts as a lubricant between the eye and eyelid. The blink mechanism replenishes the tear film as the eyelids glide over the anterior surface of the eye. Between each blink, the tear film breaks up as the surface dehydrates with air exposure. However, the placement of a CL can disrupt the integrity of the tear film, which can cause discomfort and decrease visual acuity.[167, 168] With CL wear, the tear film is split into a pre-lens tear film, which forms over the front surface of the CL, and the post-lens tear film, which forms between the lens and the cornea. Successful CL materials aim to preserve the tear film integrity by keeping the lens hydrated and providing a wettable front surface to help maintain a physiological tear break-up time (BUT), which is the time it takes for the first observable break-up in the tear film. To determine the clinical performance of a CL, it is important to assess BUT of the pre-lens tear film, which contributes to the comfort and stable visual acuity of the CL wearer.[168, 169]

BUT of the pre-lens tear film can be evaluated using several methods, which can be broadly classified into two categories, the invasive and non-invasive techniques.[169, 170] The most widely used invasive tear BUT technique is the fluorescein break-up test. This test allows the tear film to be clearly visualized with the insertion of a fluorescent dye under a highly magnified lens on the slit lamp biomicroscope. However, studies have shown that the instillation of fluorescein onto the eye can increase the total tear amount and induce reflex tear secretion, which reduces the repeatability and accuracy of BUT.[171, 172] For more reliable tear BUT results, non-invasive (NIBUT) methods can be

employed.

Several non-invasive techniques to assess BUT exist, all of which require additional clinical instruments. The most common include the Tearscope, keratometer, and corneal topographer.[170, 173] The Tearscope can be used to measure NIBUT, which is inferred from the interference patterns reflected off the tear film from a LED light source. However, the interference patterns are quite variable[174] and interpretation is subjective.[175] The keratometer allows the clinician to assess NIBUT by measuring the time elapsed for the reflected mire rings to distort on the patient's tear film.[176, 177] Similarly, the corneal topographer maps the corneal surface and measures NIBUT by assessing the distortion of placido rings reflected onto the patient's tear film.[178, 179] Compared to the keratometry, which only allows for the central 3.0-3.5 mm of the cornea to be examined, the advantage of using the corneal topographer is the wide field of view extending to the periphery of the corneal surface. This is an important aspect to consider when measuring BUT, because the tear break-up is not limited to the centre of the cornea but extends across the entire anterior surface of the eye. Hence, corneal topography was chosen in this study to measure NIBUT.

To simulate the pre-lens tear film, an *in vitro* eye model (OcuFlow II, described in the previous chapter) is used. The use of an eye model offers the advantage of CL testing *in vitro* with various controlled parameters that are otherwise not possible *in vivo*. The purpose of this chapter is to evaluate the pre-lens NIBUT of silicone hydrogels with corneal topography, using OcuFlow II to simulate CL wear.

6.2 Materials and Methods

6.2.1 Contact Lenses

Two commercially available silicone CLs (lotrafilcon B [Air Optix Aqua, Alcon, Fort Worth,

TX] and comfilcon A [Biofinity, CooperVision, Pleasanton, CA]) were evaluated. All lenses had a dioptric power of -3.00 and the lens properties are outlined in Table 6-1.

Table 6-1. Properties of silicone hydrogels used in the study.

	Air Optix Aqua™	**Biofinity™**
United States Adopted Name	lotrafilcon B	comfilcon A
Manufacturer	Alcon	CooperVision
Centre Thickness (mm)	0.08	0.08
Back Optic Zone Radius (mm)	8.6	8.6
Diameter (mm)	14.2	14.0
Water Content (%)	33	48
Oxygen Permeability ($x10^{-11}$)	110	128
Oxygen Transmissibility ($x10^{-9}$)	138	160
Surface Treatment	Plasma Coating	None
Wetting Agent	Moist agent in packaging solution (1% copolymer 845)	None
Principal Monomers	DMA + TRIS + siloxane macromer	NVP, VMA, IBM, TAIC, M3U, FM0411M, HOB

DMA, N,N-dimethylacrylamide; TRIS, trimethylsiloxy silane; NVP, N-vinyl pyrrolidone; VMA, *N*-vinyl-*N*-methylacetamide; IBM, isobornyl methacrylate; TAIC, 1,3,5-triallyl-1,3,5-triazine-2,4,6(1*H*,3*H*,5*H*)-trione; M3U, bis(methacyloyloxyethyl iminocarboxy ethyloxypropyl)-poly(dimethylsiloxane)-poly(trifluoropropylmehylsiloxane)-poly(methoxy-poly[ethyleneglycol] propylmethlsiloxane); FM0411M, methacryloyloxyethyl iminocarboxyethyloxypropyl-poly(dimethylsiloxy)-butyldimethylsilane; HOB, 2-hydroxybutyl methacrylate.

6.2.2 Artificial Tear Solution

ATS consists of various physiological tear film components, including a range of salts, proteins, and lipids. The recipe for a homogenous ATS has been previously established by our group.[148] A modified ATS was prepared in two phases separating the protein (Table 6-2) and lipid (Table 6-3) phase to allow for independent delivery of the two phases onto the eye model. Both phases were dissolved in complex salt solution (CSS) (Table 6-4). The protein phase was dissolved in CSS using a magnetic stirring bar. The lipid phase was initially dissolved in hexane ether as a four lipid stock consisting of two polar lipids and two nonpolar lipids. The lipid stock was dissolved in

CSS using a model 50D Aquasonic water bath (VWR, Radnor, PA) and the hexane ether was purged using pressured nitrogen.

Table 6-2. Protein phase of ATS.

Protein Components	mg/mL
Bovine Albumin	0.20
Bovine Submaxillary Mucin	0.15
Bovine Lactoferrin	1.80
Hen Egg Lysozyme	1.90

Table 6-3. Lipid phase of ATS.

Lipid Components	mg/mL
Cholesterol	0.00275
Cholesteryl oleate	0.03669
Phosphatidylcholine	0.01116
Phosphatidyethanolamine	0.00592

Table 6-4. Concentrated salt solution.

Salt component	mg/mL
Sodium chloride	5.26
Potassium chloride	1.19
Sodium citrate	0.44
Glucose	0.036
Urea	0.072
Calcium chloride	0.07
Sodium carbonate	1.27
Potassium hydrogen carbonate	0.30
Sodium phosphate dibasic	2.41
Hydrochloric acid	0.94
ProClin 300	0.20 µl / 1L

6.2.3 Experimental Outline

Lenses (n=4) were removed from the blister package and placed onto the corneal eye piece of OcuFlow II). The blink rate on OcuFlow II was set to 10 blinks/min and the flow rate of the protein and lipid phase were set to 6 µL/min for a total flow rate of 12 µL/min on a programmable microfluidic syringe pump (model PHD ULTRA^{TM} 4400, Harvard Apparatus, Holliston, MA). Readings were taken at 5 min, 30 min and 60 min.

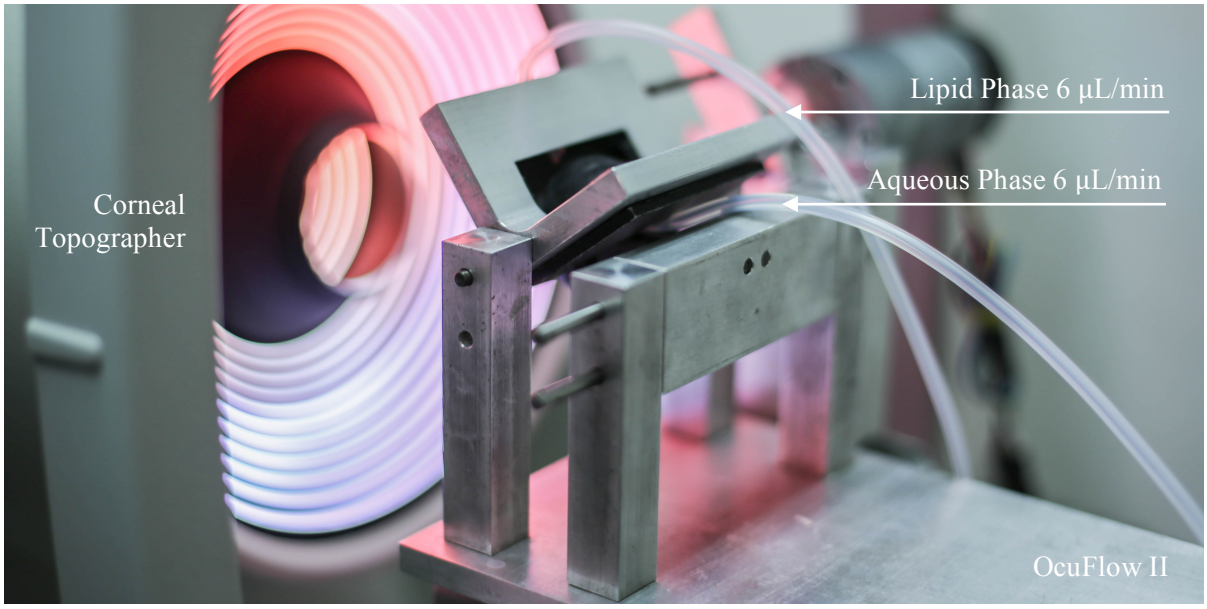

Figure 6-1. OcuFlow II mounted behind the corneal topographer for NIBUT measurements.

6.2.4 Non-invasive Tear Break-up Time

The BUT of the pre-lens tear film was measured noninvasively using a corneal topographer (Atlas 911, Zeiss Humphrey Systems, Oberkochen, Germany). The topographer assesses the tear film by reflecting a set of concentric black and white rings, known as placido rings, onto the corneal surface. To determine the pre-lens NIBUT of the CL, OcuFlow II was mounted behind the topographer (Figure 6-1) and the corneal surface was centered to the placido rings after the CL was placed on. The time taken for the first visible distortion in the placido rings was measured as the NIBUT of the pre-lens tear film.[180] Distortions in the placido ring is correlated to breaking up of the tear film. At 5 min, 30 min and 60 min, the blink mechanism on OcuFlow II was paused for 1 min and the video of the BUT recorded. The pre-lens NIBUTs were analyzed and averaged over four lenses. Unfortunately, the pre-lens NIBUT could not be evaluated on comfilcon A after 30 min and 60 min due to a looser fit of the lens on the corneal surface of the ocular pieces of OcuFlow II,

causing the lens to slide off at later time points. Thus, the pre-lens NIBUT for comfilcon A will only be reported for the shorter period of time.

6.2.5 Data Analysis

Statistical analysis was performed using Statistica 8 (StatSoft Inc., Tulsa, OK). A comparison of NIBUT between the two lens types at 5 min was conducted using a t-test. A repeated measures analysis of variance was used to determine the difference between NIBUT of lotrafilcon B at various time points.

6.3 Results

Pre-lens NIBUT varied depending on the lens type and time of measurement. For lotrafilcon B, the average pre-lens NIBUTs for the pre-lens tear film were 15.5 sec, 31.5 sec, and 18 sec at 5 min, 30 min and 60 min, respectively (Table 6-5). The average pre-lens NIBUT for comfilon A was only obtained at 5 min, which was 11.75 sec (Table 6-6). The NIBUTs for both lenses at 5 min are not significantly different ($p > 0.05$).

Table 6-5. NIBUT of lotrafilcon B (n=4) at 5 min, 30 min and 60 min of simulated CL wear using OcuFlow II.

Lotrafilcon B	5 min	30 min	60 min
Lens 1	12	33	17
Lens 2	17	32	20
Lens 3	12	35	17
Lens 4	21	26	18
Average	15.5	31.5	18
STD	4.4	3.9	1.4

Table 6-6. NIBUT of comfilcon A (n=4) at 5 min simulated CL wear using OcuFlow II.

Comfilcon A	5 min
Lens 1	14
Lens 2	13
Lens 3	11
Lens 4	9
Average	11.75
STD	2.2

The BUT was determined as the time immediately after a complete blink to the time that first distortion appeared in the placido rings, as exemplified by a lotrafilcon B lens at 17 sec (Figure 6-2.B). At time 0, the undisrupted placido rings reflected a stable tear film that was spread evenly across the surface of lotrafilcon B (Figure 6-2.A). With increased time of air exposure, there is an increase in the amount of distortion in the placido rings, which occurs due to the decreased stability of the tear film and the presence of a dry spot. The first sign of the tear film breaking up in the CL was seen at 17 sec, when the placido rings initially became distorted (Figure 6-2.B) and this time was determined to be the NIBUT. After 60 sec, the tear film was breaking up in several locations as evidenced by the increased amount of distortions throughout the placido rings (Figure 6-2.C).

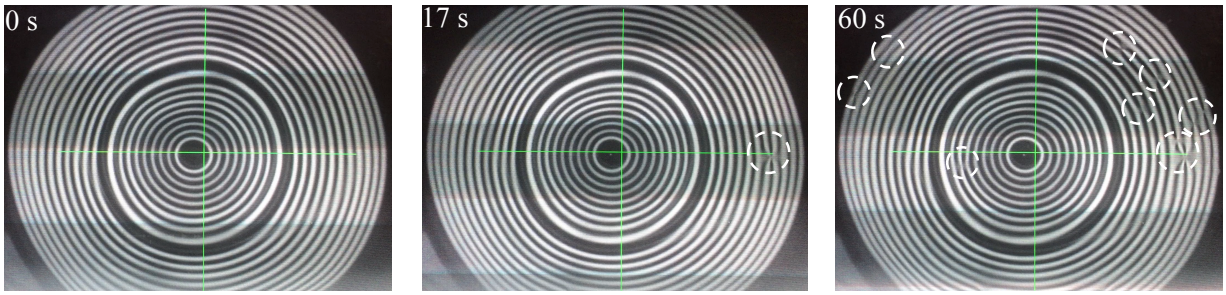

(A) (B) (C)

Figure 6-2. Topography images of a lotrafilcon B lens at 0 sec (A), 17 sec (B), and 60 sec (C) after 5 min of simulated CL wear using OcuFlow II.

At 5 mins of simulated CL wear with the comfilcon A lens, concentric placido rings were observed on the pre-lens tear film (Figure 6-3.A). Shortly beyond this time point, the placido rings were distorted around the centre as the lens started to shift (Figure 6-3.B). As time increased, the CL became more shifted, as evidenced by the significant distortion of the placido rings after 60 min (Figure 6-3.C). Comfilcon A did not withstand prolonged simulation of CL wear using OcuFlow II. Hence, reliable pre-lens NIBUT measurements were not obtained at 30 and 60 min of simulated CL wear using OcuFlow II.

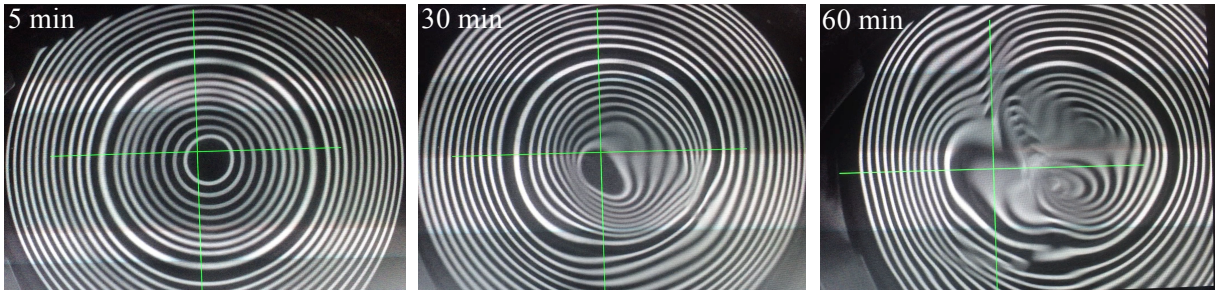

(A) (B) (C)

Figure 6-3. Topography image of a comfilcon A lens after 5 min (A), 30 min (B), and 60 min(C) of simulated CL wear using OcuFlow II.

6.4 Discussion

Two silicone hydrogels were selected for their unique surface properties. Lotrafilcon B consists of a modified surface with a hydrophilic plasma coating, which serves to increase oxygen transmissibility.[15, 151] In contrast, comfilcon A is inherently wettable and does not require surface treatment.[151, 181] The data reported suggests that the pre-lens tear film on lotrafilcon B was more stable than comfilcon A, as reflected by the longer NIBUT of 15.5 sec to 11.75 sec. On both lenses, a similar distortion pattern of tear break-up on the pre-lens tear film was observed on OcuFlow II compared to on a physiological tear film, which suggest that a similar mechanism of tear break-up is in play. The distortion pattern was observed as the contact of concentric placido rings at a point. With

increased time of air exposure, there is an increase in the amount of distortion in the placido rings, which occurs due to the decrease in the tear film stability and presence of dry spots.

Compared to clinical values (4.73 sec – 7.24 sec) of pre-lens NIBUT on lotrafilcon B,[182] the values observed on OcuFlow II were higher (12 sec - 33 sec). This can be explained by the tenfold increase in the amount of tear flow (12 µL/min) on OcuFlow II as compared to the average physiological tear flow of 1.2 µL/min.[21] 12 µL/min was determined as the minimum tear flow rate to achieve a smooth regeneration of the tear film over the surface of the CL on the current OcuFlow II platform. Notably, pre-lens NIBUTs from the clinical study[182] were measured after an extended period of continuous wear for four weeks, whereas, the pre-lens NIBUT measurements in this study were all made within the span of an hour exposure to the ATS. The time difference in CL wear may also contribute to the higher pre-lens NIBUTs observed on OcuFlow II as a result of less mechanical wear on the CL, which may affect the quality of the pre-lens tear film.

The first pre-lens NIBUT was taken at 5 min to allow for the steady flow of tear solution to rinse out any excess blister pack solution on the lens. The average NIBUT at 5 min was the lowest measurement at 15.5 sec, suggesting that the tear flow may have not completely stabilized on the OcuFlow II system. At 30 min, the pre-lens NIBUT for lotrafilcon B increased to an average measurement of 31.5 sec ($p < 0.05$). This suggests that the pre-lens tear film was the most stable at this time point, where a sufficient time period had passed to allow the tear solution to optimally equilibrate with the OcuFlow II model. Surprisingly, at 60 min, the pre-lens NIBUT dropped significantly ($p < 0.05$) to an average measurement of 18 sec. This can be attributed to the much accelerated wear and tear of the CL, due to the forces experienced through the mechanical wear of OcuFlow II as compared to physiological levels. Further research is needed to determine whether the friction and pressure exerted on the CL by the OcuFlow II system is representative of on-eye

conditions.

On the human cornea, CLs fit the corneal surface differently, depending on its shape (curvature, thickness, diameter) and material. Similarly, the different lens materials assessed in this study varied in CL fit on the *in vitro* eye model, which consisted of an eye piece with a fixed curvature. The fit and movement of the CL plays an important role in determining the stability of the pre-lens tear film. The fitting of lotrafilcon B on the corneal surface of the eye piece was ideal. Regrettably, comfilcon A did not fit the eye piece optimally. Initially, the inherent flexibility of the comfilcon A material allowed the lens to accommodate the non-ideal fit for a short period of time (Figure 6-3.A). As the lens returned to its most stable orientation, the post-lens tear film accumulated unevenly underneath the CL (Figure 6-3.B), which further exacerbated the shifting and folding of the lens (Figure 6-3.C). As a result of the lens movement, the pre-lens tear film on comfilcon A was not stable enough to obtain NIBUT measurements. The improved fit of lotrafilcon B may be due to its higher lens modulus of 1.2 MPa, which provided mechanical stability and resistance to deformation of the lens. Assorted corneal eye pieces with a range of curvatures can be designed in future iterations for proper fitting of different CLs. Furthermore, a control NIBUT value without the CL could not be obtained due to the hydrophobic property of the acetal eye piece on OcuFlow II, which did not allow the tear film to spread evenly across the corneal surface. Alternative materials with hydrophilic properties, such as agar or explanted corneal tissue, can be explored in future iterations of OcuFlow II. Detailed limitations and future work of OcuFlow II will be discussed in the next chapter.

6.5 Conclusion

Material properties, such as modulus and surface finish, of the lens play an important role in the performance of simulated CL wear. As a result of differences in the material properties of the two

silicone hydrogels, the lenses had varying pre-lens NIBUT. A faster pre-lens tear BUT occurred on comfilcon A than lotrafilcon B but only initially. In addition, a higher modulus assisted the better fit of the lotrafilcon B on the corneal surface of OcuFlow II. Results from this study demonstrates the ability of OcuFlow II in providing CL wear simulations that are reflective of the ocular environment. Future work will aim to improve reliability and versatility of OcuFlow II to accommodate various study objectives related to testing various on-eye parameters.

Chapter 7 – Limitations and Future Work of OcuFlow II Platform 2

The focus of OcuFlow II was to implement two key features, a blink mechanism and a tear film structure, to allow for more advanced CL testing. The vertical blink mechanism was achieved by enabling an upward rotational motion of the eyelid actuated by motors and a tear film was successfully generated through implementing a controlled tear fluid secretion mechanism that allowed for separate delivery of both lipid and aqueous phases. These features provided a consistent setup to evaluate CL *in vitro*, while simulating mechanical wear and physiological tear flow. In particular, a tear film over the anterior surface of eye was generated and it was validated through the consistent NIBUT seen over the surface of lotrafilcon B (Chapter 6). However, some limitations were revealed in the OcuFlow setup when different lens materials were tested. These drawbacks can be broadly broken down into two parts, relating to the mechanical setup and the ATS.

7.1 Mechanical Setup

7.1.1 Eye piece

Currently, the radius of the corneal eye piece is 9 mm, while the cornea has an average radius of curvature of 7.8 mm and most CL have a back optic zone radius less than 9 mm. As seen in the previous chapter, CLs were sensitive to this discrepancy between the radii, which affected their placement over the corneal surface of the acetal eye pieces. As a result, consistent CL testing was not possible on lenses that did not fit the curvature of the corneal surface. To address this, future eye pieces should be designed to be able to accommodate various base curves. A possible path moving forward could be exploring a flexible eyelid material to allow for wide tolerance in fitting CLs with different base curves or to design eye pieces with various curvatures.

Although acetal has a relatively wettable surface when compared to other materials explored

for the eye piece, its ability to spread ATS evenly across the surface is still inadequate compared to the corneal tissue of a human eye. In particular, the ATS could not spread across the surface of the acetal eye piece in the absence of a CL. A representative corneal surface is crucial in providing a foundation for the mixing and exchange of the post-lens tear film, which plays a key role in the behavior of tear component uptake from the posterior surface of the CL.[183, 184] To achieve this, a more hydrophilic corneal surface, synthetic tissue and *ex vivo* animal cornea could be explored in future eye pieces.

7.1.2 Eyelid Piece

The assumption made during the design phase of the eyelid piece in platform 2 is that by designing a 240 μm radius offset between the eyelid and eyeball to account for the CL and tear film thickness, the eyelid would rotate concentrically about the eye piece along its central axis. Since the eye piece consists of two spherical bodies that are off-centred from each other, the lower half of the eyelid interfered with the eye piece during blinking. As seen in Figure 7-1.A, the eyelid (blue) would collide into the corneal surface at 240 μm radius offset rotating along the same pivoting axis at the opened eyelid position. Thus, the eyelid portion below the equator was modified by increasing the clearance between the eye and eyelid to prevent the eyelid margin from interfering with the corneal surface (Figure 7-1.B).

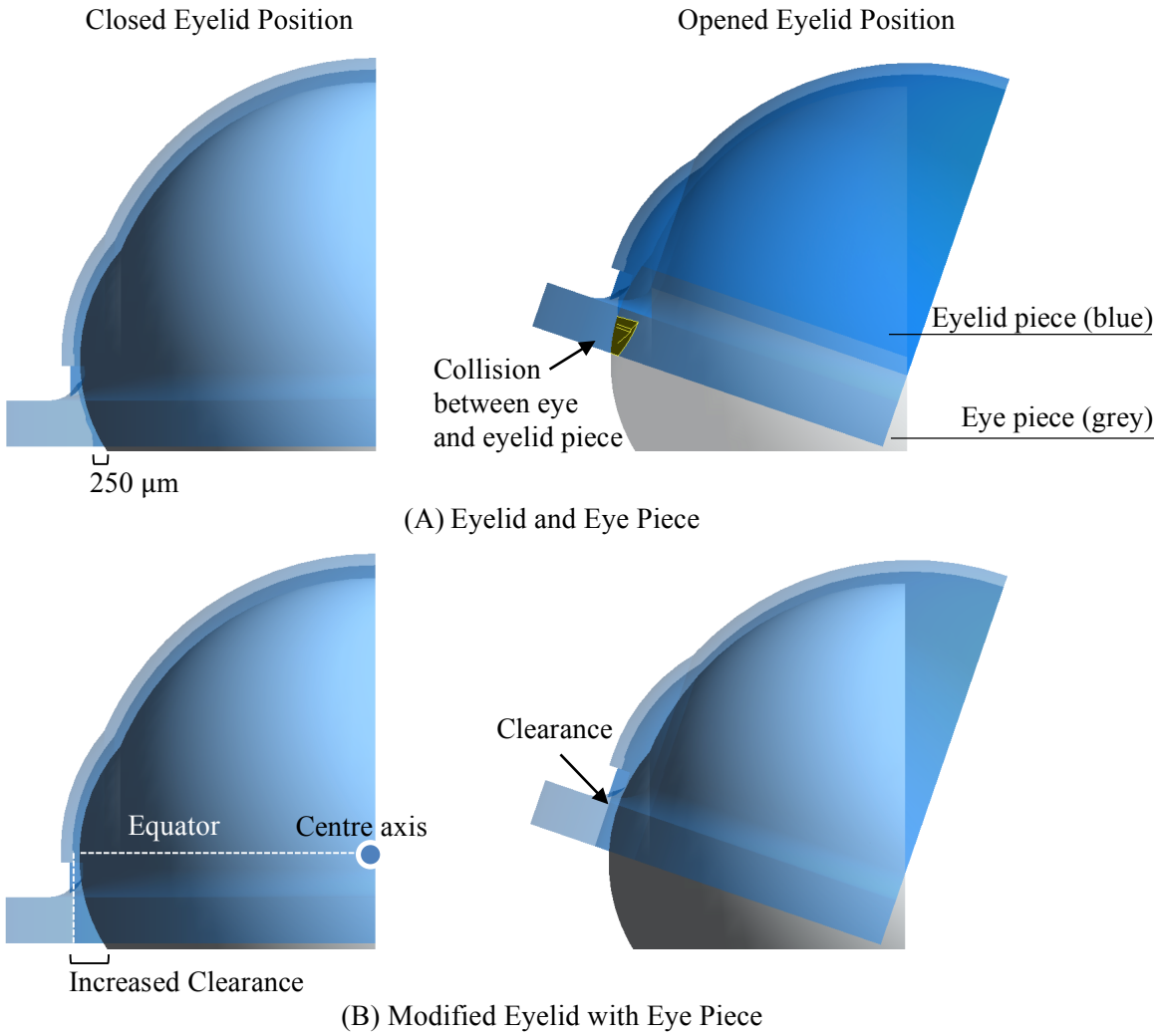

Figure 7-1. Side view profile of the original and modified eyelid design (blue) in the closed (A) and opened (B) orientation with respect to the eye piece (grey).

As a result of the modifications made on the eyelid, the increased clearance between the eye and eyelid piece prevented the necessary capillary action and surface tension required to replenish the tear film over the corneal surface. To address this, two workarounds were put in place. As implemented in chapter 6, the first adjustment involved increasing the tear volume to fill in the clearance gap. The second modification required the attachment of a soft eyelid margin extension (Figure 5-8.A) as discussed in chapter 5, which allowed for a closer and more lenient contact with the

surface of the eye, without interfering with the CL. In future designs, the shape and placement of the eyelid should follow the curvature of the eye consistently, with a tight tolerance to maintain the surface tension and pressure necessary for the generation of a stable tear film.

7.1.3 Platform

The platform enables the modeling of a representative eye and eyelid interaction mechanism, as well as the capability of delivering the protein and lipid components onto the CL. Although the basic function of the platform was achieved, improvements can be made in future iterations to increase the versatility of the model.

Eye and Eyelid Interaction

As mentioned previously, the blink motion is achieved by pivoting the eyelid piece upwards and downwards about a central axis. However, CLs with different properties may experience different pressure on the eye model, which is dictated by the trajectory of the eyelid's movement. The force applied by the eyelid can be measured using piezoresistive sensors or through a CL with internal biosensors.[185, 186] The static pressure between the eyelid and the ocular surface is estimated to be 8 mm Hg on human eyes.[185] Future iterations should aim to measure this pressure, as excess force created by the blink mechanism may induce accelerated wear and tear of the CL and the pressure may impact any drug uptake or lipid deposition. In addition, a load variable trajectory design should be considered to allow for calibration of pressures of varying CL types and experimental conditions.

Controlled Tear Flow

Currently, the tear flow mechanism relies on delivering tear solution using a microfluidic pump through silicone tubes, which have an inner diameter of 0.063 inch. This setup works well with the current flow rate and tear volume used for the protein and lipid phase. However, on the human eye, lipids are secreted in much smaller volumes through a holocrine process, which releases lipids by

rupturing the plasma membrane of holocrine tissues.[187, 188] The lipid phase and its delivery mechanism should be fine-tuned in future iterations to account for volume and consistency of the lipid phase, which plays an important role in establishing a stable layered structure of the tear film.[39] Moreover, a holocrine mode of secretion can be mimicked using osmotic pumps, which allow for precise delivery of small volumes - but highly concentrated doses - of lipids.

7.2 Artificial Tear Solution

Although, a smooth tear film was achieved in the system, as evidenced by the concentric placido rings observed while measuring NIBUT of the CL (Chapter 6), it is unclear whether a bilayered structure was generated. Making up the bulk of both the protein and lipid phases, the aqueous layer was undeniably present. However, the existence of a stable lipid layer is more ambiguous. In an attempt to identify the tear lipid layer, lipid and protein solutions (as described in Chapter 6) were infused onto the corneal surface of the eye model and visualized using a TearScope. Interference fringes were not observed with and without a CL mounted, which suggests the absence of a stable lipid layer. This result is not surprising, considering the lipid phase was forcefully dissolved in aqueous CSS by sonication. The aqueous phase may disrupt the necessary and intricate interaction between different lipids to maintain the structural integrity of the lipid layer.[39] In order to simulate a representative lipid layer, a new lipid phase with alternative solvent, additional lipids, and varying levels of concentration needs to be devised.

7.3 Future Work

The creation of a comprehensive *in vitro* eye model is an iterative process and requires redesign and validation through the progression of each development phase. Future work aims to enhance the material, structure, and fit of the eye and eyelid pieces. To increase the versatility of the model, an

upgrade to the platform should be considered to allow for controlled blink pressure and a more representative mechanism of lipid secretion. In addition, a physiologically relevant formulation should be developed for the lipid phase to enable the generation of a stable tear lipid layer. Future models can be validated for CL testing through various approaches, such as evaluating BUT, tear film quality, lens deposition, and blink pressure. Results from both the *in vitro* eye model and *in vivo* studies can be compared to deepen our current understanding and elucidate new findings on how CL interact with the ocular surface.

Chapter 8 – General Discussion

This thesis provided insight on how cholesteryl esters interact with various CL materials. Although the amount of lipid deposition has been explored by several groups, the location of lipid deposition, particularly on silicone hydrogels remains unclear. Hence, an *in vitro* eye model was constructed with the intent to better understand lipid deposition patterns under physiologically relevant conditions. The findings on lipid deposition and the development of the *in vitro* eye model are summarized in the following sections.

Results from Chapter 3 showed that the location of fluorescently tagged cholesteryl ester deposits was highly influenced by the lens property. Lenses containing NVP and PVP showed a strong attraction of cholesteryl ester into the lens matrix. Lenses with surface treatments deterred cholesteryl ester deposition to the bulk of the lens for the first 14 days and mainly deposited on the surfaces. This suggests that surface properties may play a bigger role in reducing lipid deposition than bulk polymeric composition. However, regardless of the type of silicone hydrogel tested, the amount of lipids deposited increased over time. This finding correlates with the lower overall satisfaction with increased wear time seen in a previous clinical study that simultaneously evaluated comfort and lipid deposition.[74] To avoid the buildup of deposits over time and reduce deposition related complications, daily disposable lenses have been shown to be effective at combating discomfort.[116, 120, 189] Therefore, wear modality is particularly important to consider in patients with lipid related conditions, such as meibomian gland dysfunction and evaporative dry eye. However, patients that are less sensitive to the accumulation of lipid may choose a wear schedule with less frequency of replacement. Hence, practitioners should consider different wear modalities and lens materials to optimize patient comfort.

To test the clinical relevance of results found in Chapter 3, an *in vitro* eye model was

developed and described in Chapters 4 and 5. The model was able to achieve a vertical blink motion, which simulated deposition patterns on the lens with mechanical wear. Previous evidence suggested that wearing a lens with a lower coefficient of friction can improve comfort.[119] In addition to the physical pressures applied on the eye, it is likely that forces acting on the CL may play a role in lipid deposition and indirectly affect comfort. Aside from a representative blink motion, another feature implemented into this model was the tear film structure. This was enabled by introducing a tear flow system onto the ocular surface with separate delivery inputs for the aqueous and lipid phases. In Chapter 6, the blink mechanism and tear film was validated by measuring the pre-lens tear BUT. The results demonstrated successful tear films were created, but it was lacking in flexibility to accommodate different lens types.

The interaction of various tear film components on different CL materials is highly complex. The presence of uncontrolled and confounding variables with human subjects do not help to simplify the problem. To complement results obtained *in vivo*, *in vitro* models allow for isolation of individual variables, which helps to pinpoint factors contributing to changes in lens material and its interaction with the ocular environment, all of which are factors that may affect CL comfort. However, models are designed to mimic rather than to replicate the physiological condition, and it is important to understand the advantages and limitations of each system.

The *in vitro* testing method employed should be tailored, depending on the purpose of the experiment. A simple vial model serves as a great method for comparing the relative quantity of lipid deposition between different CLs, which is sufficient at mirroring results seen *in vivo*. However, to explore a more complex mechanism such as the location of lipid deposits on various lens types, a more sophisticated *in vitro* eye model is required to fully account for the various factors at play. Ultimately, the end goal is to understand lipid deposition that is reflective of on eye conditions and

obtain clinically relevant results.

In conclusion, lipid deposition is greatly impacted by the lens property and a better understanding of how lipid deposition affects comfort can be explored by using an *in vitro* simulation of CL wear. Findings from this thesis paved the path for a more reliable CL testing method to keep up with the increasing demand for novel materials with enhanced comfort.

Bibliography

1. Heitz RF, Enoch JM *Leonardo da Vinci: An assessment on his discourses on image formation in the eye*. Springer-Verlag: New York; 1987.

2. Key JE. Development of contact lenses and their worldwide use. *Eye Contact Lens* 2007; **33**(6 Pt 2)**:** 343-345; discussion 362-343.

3. Nichols JJ, Willcox MD, Bron AJ, Belmonte C, Ciolino JB, Craig JP *et al.* The TFOS International Workshop on Contact Lens Discomfort: executive summary. *Invest Ophthalmol Vis Sci* 2013; **54**(11)**:** TFOS7-TFOS13.

4. Riley C, Chalmers RL. Survey of contact lens-wearing habits and attitudes toward methods of refractive correction: 2002 versus 2004. *Optom Vis Sci* 2005; **82**(6)**:** 555-561.

5. Morgan P, Woods C, Tranoudis I, Helland M, Efron N, Grupcheva C *et al.* International contact lens prescribing in 2011. *Contact Lens Spectrum* 2012; **27**(January 2012)**:** 26-32.

6. Wichterle O, Lim D. Hydrophilic Gels for Biological Use. *Nature* 1960; **185**(4706)**:** 117-118.

7. Bennett ES, Weissman BA *Clinical Contact Lens Practice*. Lippincott Williams & Wilkins; 2005.

8. Holden BA, Mertz GW. Critical oxygen levels to avoid corneal edema for daily and extended wear contact lenses. *Invest Ophthalmol Vis Sci* 1984; **25**(10)**:** 1161-1167.

9. Young MD, Benjamin WJ. Calibrated oxygen permeability of 35 conventional hydrogel materials and correlation with water content. *Eye Contact Lens* 2003; **29**(2)**:** 126-133.

10. Polse KA, Brand RJ, Cohen SR, Guillon M. Hypoxic effects on corneal morphology and function. *Invest Ophthalmol Vis Sci* 1990; **31**(8)**:** 1542-1554.

11. Brennan NA, Coles ML. Extended wear in perspective. *Optom Vis Sci* 1997; **74**(8)**:** 609-623.

12. Safvati A, Cole N, Hume E, Willcox M. Mediators of neovascularization and the hypoxic cornea. *Curr Eye Res* 2009; **34**(6)**:** 501-514.

13. Sweeney DF, Holden BA. Silicone elastomer lens wear induces less overnight corneal edema than sleep without lens wear. *Curr Eye Res* 1987; **6**(12)**:** 1391-1394.

14. Fanti P. Silicone contact lens wear III. Physiology of poor tolerance. *Contact Intraocul Lens Med J* 1980; **6:** 111-119.

15. Nicolson PC, Vogt J. Soft contact lens polymers: an evolution. *Biomaterials* 2001; **22**(24)**:** 3273-3283.

16. Tighe BJ. A decade of silicone hydrogel development: surface properties, mechanical

properties, and ocular compatibility. *Eye Contact Lens* 2013; **39**(1)**:** 4-12.

17. Craig J. Structure and function of the preocular tear film. In the tear film: structure, function and clinical examination. 2002**:** 18-50.

18. King-Smith PE, Fink BA, Fogt N, Nichols KK, Hill RM, Wilson GS. The thickness of the human precorneal tear film: evidence from reflection spectra. *Invest Ophthalmol Vis Sci* 2000; **41**(11)**:** 3348-3359.

19. Wang J, Fonn D, Simpson TL, Jones L. Precorneal and pre- and postlens tear film thickness measured indirectly with optical coherence tomography. *Invest Ophthalmol Vis Sci* 2003; **44**(6)**:** 2524-2528.

20. Dartt DA, Willcox MD. Complexity of the tear film: importance in homeostasis and dysfunction during disease. *Exp Eye Res* 2013; **117:** 1-3.

21. Mishima S, Gasset A, Klyce SD, Jr., Baum JL. Determination of tear volume and tear flow. *Invest Ophthalmol* 1966; **5**(3)**:** 264-276.

22. Wolff E. The mucocutaneous junction of the lid margin and the distribution of the tear fluid. *Trans Ophthalmol Soc UK* 1946; **66:** 291-308.

23. IK G. Distribution of mucins at the ocular surface. *Exp Eye Res* 2004; **78**(3)**:** 379-388.

24. Botelho SY. Tears and the Lacrimal Gland. *Sci Am* 1964; **211:** 78-86.

25. Hodges RR, Dartt DA. Tear film mucins: front line defenders of the ocular surface; comparison with airway and gastrointestinal tract mucins. *Exp Eye Res* 2013; **117:** 62-78.

26. Tiffany JM. Composition and biophysical properties of the tear film: knowledge and uncertainty. *Adv Exp Med Biol* 1994; **350:** 231-238.

27. Hollingsworth MA, Swanson BJ. Mucins in cancer: protection and control of the cell surface. *Nat Rev Cancer* 2004; **4**(1)**:** 45-60.

28. Molloy MP, Bolis S, Herbert BR, Ou K, Tyler MI, van Dyk DD *et al.* Establishment of the human reflex tear two-dimensional polyacrylamide gel electrophoresis reference map: new proteins of potential diagnostic value. *Electrophoresis* 1997; **18**(15)**:** 2811-2815.

29. de Souza GA, Godoy LM, Mann M. Identification of 491 proteins in the tear fluid proteome reveals a large number of proteases and protease inhibitors. *Genome Biol* 2006; **7**(8)**:** R72.

30. Zhou L, Roger W, Foo Y, Liu S, Leonard P, Donald T. Characterisation of human tear proteins using high-resolution mass spectrometry. *Ann Acad Med Singapore* 2006; **35:** 400-407.

31. Carnt N. The TFOS 8th International Conference on the Tear Film & Ocular Surface: Basic

Science and Clinical Relevance (Montpellier, France, September 7-10, 2016). Highlights from the Platform Sessions. *Ocul Surf* 2017; **15**(2)**:** 257-263.

32. Broekhuyse RM. Tear lactoferrin: a bacteriostatic and complexing protein. *Invest Ophthalmol* 1974; **13**(7)**:** 550-554.

33. Flanagan JL, Willcox MD. Role of lactoferrin in the tear film. *Biochimie* 2009; **91**(1)**:** 35-43.

34. Willcox MD, Lan J. Secretory immunoglobulin A in tears:functions and changes during contact lens wear. *Clin Exp Optom* 1999; **82**(1)**:** 1-3.

35. Runstrom G, Mann A, Tighe B. The fall and rise of tear albumin levels: a multifactorial phenomenon. *Ocul Surf* 2013; **11**(3)**:** 165-180.

36. Wolff E *The Anatomy of the Eye and Orbit, fourth ed*. H.K. Lewis and Co: London; 1954.

37. Bron AJ, Tiffany JM. The meibomian glands and tear film lipids. Structure, function, and control. *Adv Exp Med Biol* 1998; **438:** 281-295.

38. McDonald JE. Surface phenomena of tear films. *Trans Am Ophthalmol Soc* 1968; **66:** 905-939.

39. Bron AJ, Tiffany JM, Gouveia SM, Yokoi N, Voon LW. Functional aspects of the tear film lipid layer. *Exp Eye Res* 2004; **78**(3)**:** 347-360.

40. Shine WE, McCulley JP. Polar lipids in human meibomian gland secretions. *Curr Eye Res* 2003; **26**(2)**:** 89-94.

41. Greiner JV, Glonek T, Korb DR, Leahy CD. Meibomian gland phospholipids. *Curr Eye Res* 1996; **15**(4)**:** 371-375.

42. Craig JP, Tomlinson A. Importance of the lipid layer in human tear film stability and evaporation. *Optom Vis Sci* 1997; **74**(1)**:** 8-13.

43. McCulley JP, Shine WE. Eyelid disorders: the meibomian gland, blepharitis, and contact lenses. *Eye Contact Lens* 2003; **29**(1 Suppl)**:** S93-95; discussion S115-118, S192-114.

44. McCulley JP, Shine W. A compositional based model for the tear film lipid layer. *Trans Am Ophthalmol Soc* 1997; **95:** 79-88; discussion 88-93.

45. Ginsburg GS, Atkinson D, Small DM. Physical properties of cholesteryl esters. *Prog Lipid Res* 1984; **23**(3)**:** 135-167.

46. Butovich IA. Cholesteryl esters as a depot for very long chain fatty acids in human meibum. *J Lipid Res* 2009; **50**(3)**:** 501-513.

47. Nichols JJ, King-Smith PE. Thickness of the pre- and post-contact lens tear film measured in

vivo by interferometry. *Invest Ophthalmol Vis Sci* 2003; **44**(1)**:** 68-77.

48. Fonn D, Dumbleton K. Dryness and discomfort with silicone hydrogel contact lenses. *Eye Contact Lens* 2003; **29**(1 Suppl)**:** S101-104; discussion S115-108, S192-104.

49. Fonn D. Targeting contact lens induced dryness and discomfort: what properties will make lenses more comfortable. *Optom Vis Sci* 2007; **84**(4)**:** 279-285.

50. Martin R, Sanchez I, de la Rosa C, de Juan V, Rodriguez G, de Paz I *et al.* Differences in the daily symptoms associated with the silicone hydrogel contact lens wear. *Eye Contact Lens* 2010; **36**(1)**:** 49-53.

51. Gellatly KW, Brennan NA, Efron N. Visual decrement with deposit accumulation of HEMA contact lenses. *Am J Optom Physiol Opt* 1988; **65**(12)**:** 937-941.

52. Sack RA, Jones B, Antignani A, Libow R, Harvey H. Specificity and biological activity of the protein deposited on the hydrogel surface. Relationship of polymer structure to biofilm formation. *Invest Ophthalmol Vis Sci* 1987; **28**(5)**:** 842-849.

53. Leahy CD, Mandell RB, Lin ST. Initial in vivo tear protein deposition on individual hydrogel contact lenses. *Optom Vis Sci* 1990; **67**(7)**:** 504-511.

54. Minno GE, Eckel L, Groemminger S, Minno B, Wrzosek T. Quantitative analysis of protein deposits on hydrophilic soft contact lenses: I. Comparison to visual methods of analysis. II. Deposit variation among FDA lens material groups. *Optom Vis Sci* 1991; **68**(11)**:** 865-872.

55. Carney FP, Morris CA, Willcox MD. Effect of hydrogel lens wear on the major tear proteins during extended wear. *Aust N Z J Ophthalmol* 1997; **25 Suppl 1:** S36-38.

56. Garrett Q, Chatelier RC, Griesser HJ, Milthorpe BK. Effect of charged groups on the adsorption and penetration of proteins onto and into carboxymethylated poly(HEMA) hydrogels. *Biomaterials* 1998; **19**(23)**:** 2175-2186.

57. Jones L, Senchyna M, Glasier MA, Schickler J, Forbes I, Louie D *et al.* Lysozyme and lipid deposition on silicone hydrogel contact lens materials. *Eye Contact Lens* 2003; **29**(1 Suppl)**:** S75-79; discussion S83-74, S192-194.

58. Chow LM, Subbaraman LN, Sheardown H, Jones L. Kinetics of in vitro lactoferrin deposition on silicone hydrogel and FDA group II and group IV hydrogel contact lens materials. *J Biomater Sci Polym Ed* 2009; **20**(1)**:** 71-82.

59. Ng A, Heynen M, Luensmann D, Jones L. Impact of tear film components on lysozyme deposition to contact lenses. *Optom Vis Sci* 2012; **89**(4)**:** 392-400.

60. Subbaraman LN, Glasier MA, Senchyna M, Sheardown H, Jones L. Kinetics of in vitro lysozyme deposition on silicone hydrogel, PMMA, and FDA groups I, II, and IV contact lens

materials. *Curr Eye Res* 2006; **31**(10)**:** 787-796.

61. Bontempo AR, Rapp J. Protein-lipid interaction on the surface of a hydrophilic contact lens in vitro. *Curr Eye Res* 1997; **16**(8)**:** 776-781.

62. Carney FP, Morris CA, Milthorpe B, Flanagan JL, Willcox MD. In vitro adsorption of tear proteins to hydroxyethyl methacrylate-based contact lens materials. *Eye Contact Lens* 2009; **35**(6)**:** 320-328.

63. Suwala M, Glasier MA, Subbaraman LN, Jones L. Quantity and conformation of lysozyme deposited on conventional and silicone hydrogel contact lens materials using an in vitro model. *Eye Contact Lens* 2007; **33**(3)**:** 138-143.

64. Subbaraman LN, Jones L. Kinetics of lysozyme activity recovered from conventional and silicone hydrogel contact lens materials. *J Biomater Sci Polym Ed* 2010; **21**(3)**:** 343-358.

65. Senchyna M, Jones L, Louie D, May C, Forbes I, Glasier MA. Quantitative and conformational characterization of lysozyme deposited on balafilcon and etafilcon contact lens materials. *Curr Eye Res* 2004; **28**(1)**:** 25-36.

66. Subbaraman LN, Glasier MA, Varikooty J, Srinivasan S, Jones L. Protein deposition and clinical symptoms in daily wear of etafilcon lenses. *Optom Vis Sci* 2012; **89**(10)**:** 1450-1459.

67. Skotnitsky C, Sankaridurg PR, Sweeney DF, Holden BA. General and local contact lens induced papillary conjunctivitis (CLPC). *Clin Exp Optom* 2002; **85**(3)**:** 193-197.

68. Skotnitsky CC, Naduvilath TJ, Sweeney DF, Sankaridurg PR. Two presentations of contact lens-induced papillary conjunctivitis (CLPC) in hydrogel lens wear: local and general. *Optom Vis Sci* 2006; **83**(1)**:** 27-36.

69. Hart DE, Tidsale RR, Sack RA. Origin and composition of lipid deposits on soft contact lenses. *Ophthalmology* 1986; **93**(4)**:** 495-503.

70. Bowers RW, Tighe BJ. Studies of the ocular compatibility of hydrogels. White spot deposits--incidence of occurrence, location and gross morphology. *Biomaterials* 1987; **8**(2)**:** 89-93.

71. Franklin V, Evans K, Jones L, Tighe B. Interaction of tear lipids with soft contact lenses. *Optom Vis Sci* 1995; **72:** 145.

72. Rapp J, Broich JR. Lipid deposits on worn soft contact lenses. *CLAO J* 1984; **10**(3)**:** 235-239.

73. Tighe BJ, Jones L, Evans K, Franklin V. Patient-dependent and material-dependent factors in contact lens deposition processes. *Adv Exp Med Biol* 1998; **438:** 745-751.

74. Jones L, Franklin V, Evans K, Sariri R, Tighe B. Spoilation and clinical performance of monthly vs. three monthly Group II disposable contact lenses. *Optom Vis Sci* 1996; **73**(1)**:**

16-21.

75. Jones L, Evans K, Sariri R, Franklin V, Tighe B. Lipid and protein deposition of N-vinyl pyrrolidone-containing group II and group IV frequent replacement contact lenses. *CLAO J* 1997; **23**(2)**:** 122-126.

76. Maissa C, Franklin V, Guillon M, Tighe B. Influence of contact lens material surface characteristics and replacement frequency on protein and lipid deposition. *Optom Vis Sci* 1998; **75**(9)**:** 697-705.

77. Pucker AD, Thangavelu M, Nichols JJ. In vitro lipid deposition on hydrogel and silicone hydrogel contact lenses. *Invest Ophthalmol Vis Sci* 2010; **51**(12)**:** 6334-6340.

78. Lorentz H, Heynen M, Trieu D, Hagedorn SJ, Jones L. The impact of tear film components on in vitro lipid uptake. *Optom Vis Sci* 2012; **89**(6)**:** 856-867.

79. Lorentz H, Jones L. Lipid deposition on hydrogel contact lenses: how history can help us today. *Optom Vis Sci* 2007; **84**(4)**:** 286-295.

80. Maziarz EP, Stachowski MJ, Liu XM, Mosack L, Davis A, Musante C *et al.* Lipid deposition on silicone hydrogel lenses, part I: quantification of oleic Acid, oleic Acid methyl ester, and cholesterol. *Eye Contact Lens* 2006; **32**(6)**:** 300-307.

81. Iwata M, Ohno S, Kawai T, Ichijima H, Cavanagh HD. In vitro evaluation of lipids adsorbed on silicone hydrogel contact lenses using a new gas chromatography/mass spectrometry analytical method. *Eye Contact Lens* 2008; **34**(5)**:** 272-280.

82. Carney FP, Nash WL, Sentell KB. The adsorption of major tear film lipids in vitro to various silicone hydrogels over time. *Invest Ophthalmol Vis Sci* 2008; **49**(1)**:** 120-124.

83. Pucker AD, Thangavelu M, Nichols JJ. Enzymatic quantification of cholesterol and cholesterol esters from silicone hydrogel contact lenses. *Invest Ophthalmol Vis Sci* 2010; **51**(6)**:** 2949-2954.

84. Lorentz H, Rogers R, Jones L. The impact of lipid on contact angle wettability. *Optom Vis Sci* 2007; **84**(10)**:** 946-953.

85. Tighe B, Franklin V, Tonge S. Contact lens care. Part 3: Contact lens material and their interaction with tears. *Optician* 2001; **221:** 22-28

.

86. Saville JT, Zhao Z, Willcox MD, Blanksby SJ, Mitchell TW. Detection and quantification of tear phospholipids and cholesterol in contact lens deposits: the effect of contact lens material and lens care solution. *Invest Ophthalmol Vis Sci* 2010; **51**(6)**:** 2843-2851.

87. Zhao Z, Carnt NA, Aliwarga Y, Wei X, Naduvilath T, Garrett Q *et al.* Care regimen and lens

material influence on silicone hydrogel contact lens deposition. *Optom Vis Sci* 2009; **86**(3)**:** 251-259.

88. Heynen M, Lorentz H, Srinivasan S, Jones L. Quantification of non-polar lipid deposits on senofilcon a contact lenses. *Optom Vis Sci* 2011; **88**(10)**:** 1172-1179.

89. Babaei Omali N, Zhu H, Zhao Z, Ozkan J, Xu B, Borazjani R *et al.* Effect of cholesterol deposition on bacterial adhesion to contact lenses. *Optom Vis Sci* 2011; **88**(8)**:** 950-958.

90. Cheung SW, Cho P, Chan B, Choy C, Ng V. A comparative study of biweekly disposable contact lenses: silicone hydrogel versus hydrogel. *Clin Exp Optom* 2007; **90**(2)**:** 124-131.

91. Zhao Z, Naduvilath T, Flanagan JL, Carnt NA, Wei X, Diec J *et al.* Contact lens deposits, adverse responses, and clinical ocular surface parameters. *Optom Vis Sci* 2010; **87**(9)**:** 669-674.

92. . Could lipid deposition on contact lenses be beneficial. *British Contact Lens Association Annual Meeting 2014*; Birmingham UK2014.

93. Hart DE, Lane BC, Josephson JE, Tisdale RR, Gzik M, Leahy R *et al.* Spoilage of hydrogel contact lenses by lipid deposits. Tear-film potassium depression, fat, protein, and alcohol consumption. *Ophthalmology* 1987; **94**(10)**:** 1315-1321.

94. Gilbard JP, Gray KL, Rossi SR. A proposed mechanism for increased tear-film osmolarity in contact lens wearers. *Am J Ophthalmol* 1986; **102**(4)**:** 505-507.

95. Lawin-Brussel CA, Refojo MF, Leong FL, Kenyon KR. Scanning electron microscopy of the early host inflammatory response in experimental Pseudomonas keratitis and contact lens wear. *Cornea* 1995; **14**(4)**:** 355-359.

96. McCanna DJ, Driot JY, Hartsook R, Ward KW. Rabbit models of contact lens--associated corneal hypoxia: a review of the literature. *Eye Contact Lens* 2008; **34**(3)**:** 160-165.

97. Chhabra M, Prausnitz JM, Radke CJ. Modeling corneal metabolism and oxygen transport during contact lens wear. *Optom Vis Sci* 2009; **86**(5)**:** 454-466.

98. Brazel CS, Peppas NA. Modeling of drug release from swellable polymers. *Eur J Pharm Biopharm* 2000; **49**(1)**:** 47-58.

99. Lin CC, Metters AT. Hydrogels in controlled release formulations: network design and mathematical modeling. *Adv Drug Deliv Rev* 2006; **58**(12-13)**:** 1379-1408.

100. Hall B, Jones LW, Forrest JA. Competitive Effects from an Artificial Tear Solution to Protein Adsorption. *Optom Vis Sci* 2015; **92**(7)**:** 781-789.

101. Keith D, Hong B, Christensen M. A novel procedure for the extraction of protein deposits from

soft hydrophilic contact lenses for analysis. *Curr Eye Res* 1997; **16**(5)**:** 503-510.

102. Hall B, Phan CM, Subbaraman L, Jones LW, Forrest J. Extraction versus in situ techniques for measuring surface-adsorbed lysozyme. *Optom Vis Sci* 2014; **91**(9)**:** 1062-1070.

103. Okada E, Matsuda T, Yokoyama T, Okuda K. Lysozyme penetration in group IV soft contact lenses. *Eye Contact Lens* 2006; **32**(4)**:** 174-177.

104. Teichroeb JH, Forrest JA, Ngai V, Martin JW, Jones L, Medley J. Imaging protein deposits on contact lens materials. *Optom Vis Sci* 2008; **85**(12)**:** 1151-1164.

105. Walther H, Lorentz H, Heynen M, Kay L, Jones LW. Factors that influence in vitro cholesterol deposition on contact lenses. *Optom Vis Sci* 2013; **90**(10)**:** 1057-1065.

106. Peng CC, Fajardo NP, Razunguzwa T, Radke CJ. In Vitro Spoilation of Silicone-Hydrogel Soft Contact Lenses in a Model-Blink Cell. *Optom Vis Sci* 2015; **92**(7)**:** 768-780.

107. Pucker AD, Nichols JJ. A method of imaging lipids on silicone hydrogel contact lenses. *Optom Vis Sci* 2012; **89**(5)**:** E777-787.

108. Jacob JT, Levet J, Jr., Edwards TA, Dassanayake N, Ketelson H. Visualizing hydrophobic domains in silicone hydrogel lenses with Sudan IV. *Invest Ophthalmol Vis Sci* 2012; **53**(7)**:** 3473-3480.

109. Jacob J, Frederick R, Tucker C, Love L. Effect of static and non-static in-vitro techniques on lipid penetration into SiHy contact lenses. *Invest Ophthalmol* 2013; **54:** 5486.

110. Mirejovsky D, Patel AS, Rodriguez DD, Hunt TJ. Lipid adsorption onto hydrogel contact lens materials. Advantages of Nile red over oil red O in visualization of lipids. *Optom Vis Sci* 1991; **68**(11)**:** 858-864.

111. Ali M, Horikawa S, Venkatesh S, Saha J, Hong JW, Byrne ME. Zero-order therapeutic release from imprinted hydrogel contact lenses within in vitro physiological ocular tear flow. *J Control Release* 2007; **124**(3)**:** 154-162.

112. Lorentz H, Heynen M, Khan W, Trieu D, Jones L. The impact of intermittent air exposure on lipid deposition. *Optom Vis Sci* 2012; **89**(11)**:** 1574-1581.

113. Phan CM, Walther H, Gao H, Rossy J, Subbaraman LN, Jones L. Development of an In Vitro Ocular Platform to Test Contact Lenses. *J Vis Exp* 2016(110)**:** e53907.

114. Furukawa RE, Polse KA. Changes in tear flow accompanying aging. *Am J Optom Physiol Opt* 1978; **55**(2)**:** 69-74.

115. Walther H, Phan CM, Subbaraman L, Jones L. Cholesterol Penetration into Daily Disposable Contact Lenses Using a Novel In Vitro Eye-Blink Model. *Invest Ophthalmol Vis Sci* 2016;

57(12)**:** 1476.

116. Nilsson SEG, Soderqvist M. Clinical performance of a daily disposable contact lens: a 3-month prospective study. *Cont Lens Anterior Eye* 1995; **18:** 81-86.

117. Brennan NA. Contact lens based correlates of soft lens wearing comfort. *Optom Vis Sci* 2009; **86**(e-abstract)**:** 90957.

118. Coles CML, Brennan NA. Coefficient of friction and soft contact lens comfort. *Optom Vis Sci* 2012; **88**(e-abstract)**:** 125603.

119. Jones L, Brennan NA, Gonzalez-Meijome J, Lally J, Maldonado-Codina C, Schmidt TA *et al.* The TFOS International Workshop on Contact Lens Discomfort: report of the contact lens materials, design, and care subcommittee. *Invest Ophthalmol Vis Sci* 2013; **54**(11)**:** TFOS37-70.

120. Lazon de la Jara P, Papas E, Diec J, Naduvilath T, Willcox MD, Holden BA. Effect of lens care systems on the clinical performance of a contact lens. *Optom Vis Sci* 2013; **90**(4)**:** 344-350.

121. Nash WL, Gabriel MM. Ex vivo analysis of cholesterol deposition for commercially available silicone hydrogel contact lenses using a fluorometric enzymatic assay. *Eye Contact Lens* 2014; **40**(5)**:** 277-282.

122. Wedler FC. Analysis of biomaterials deposited on soft contact lenses. *J Biomed Mater Res* 1977; **11**(4)**:** 525-535.

123. Hosaka S, Ozawa H, Tanzawa H, Ishida H, Yoshimura K, Momose T *et al.* Analysis of deposits on high water content contact lenses. *J Biomed Mater Res* 1983; **17**(2)**:** 261-274.

124. Castillo EJ, Koenig JL, Anderson JM, Lo J. Protein adsorption on hydrogels. II. Reversible and irreversible interactions between lysozyme and soft contact lens surfaces. *Biomaterials* 1985; **6**(5)**:** 338-345.

125. Bilbaut T, Gachon AM, Dastugue B. Deposits on soft contact lenses. Electrophoresis and scanning electron microscopic examinations. *Exp Eye Res* 1986; **43**(2)**:** 153-165.

126. Lin ST, Mandell RB, Leahy CD, Newell JO. Protein accumulation on disposable extended wear lenses. *CLAO J* 1991; **17**(1)**:** 44-50.

127. Yan G, Nyquist G, Caldwell KD, Payor R, McCraw EC. Quantitation of total protein deposits on contact lenses by means of amino acid analysis. *Invest Ophthalmol Vis Sci* 1993; **34**(5)**:** 1804-1813.

128. Meadows DL, Paugh JR. Use of confocal microscopy to determine matrix and surface protein deposition profiles in hydrogel contact lenses. *CLAO J* 1994; **20**(4)**:** 237-241.

129. Luensmann D, Zhang F, Subbaraman L, Sheardown H, Jones L. Localization of lysozyme sorption to conventional and silicone hydrogel contact lenses using confocal microscopy. *Curr Eye Res* 2009; **34**(8)**:** 683-697.

130. Panaser A, Tighe BJ. Evidence of lipid degradation during overnight contact lens wear: gas chromatography mass spectrometry as the diagnostic tool. *Invest Ophthalmol Vis Sci* 2014; **55**(3)**:** 1797-1804.

131. Schuett BS, Millar TJ. An Experimental Model to Study the Impact of Lipid Oxidation on Contact Lens Deposition In Vitro. *Curr Eye Res* 2017**:** 1-8.

132. Bontempo AR, Rapp J. Protein and lipid deposition onto hydrophilic contact lenses in vivo. *CLAO J* 2001; **27**(2)**:** 75-80.

133. Young G, Bowers R, Hall B, Port M. Clinical comparison of Omafilcon A with four control materials. *CLAO J* 1997; **23**(4)**:** 249-258.

134. Prager MD, Quintana RP. Radiochemical studies on contact lens soilation. I. Lens uptake of 14C-lysozyme from simple and complex artificial tear solutions. *J Biomed Mater Res* 1997; **36**(1)**:** 119-124.

135. Prager MD, Quintana RP. Radiochemical studies on contact lens soilation. II. Lens uptake of cholesteryl oleate and dioleoyl phosphatidylcholine. *J Biomed Mater Res* 1997; **37**(2)**:** 207-211.

136. Garrett Q, Garrett RW, Milthorpe BK. Lysozyme sorption in hydrogel contact lenses. *Invest Ophthalmol Vis Sci* 1999; **40**(5)**:** 897-903.

137. Berry M, Harris A, Corfield AP. Patterns of mucin adherence to contact lenses. *Invest Ophthalmol Vis Sci* 2003; **44**(2)**:** 567-572.

138. Guillon M, Maissa C. Contact lens wear affects tear film evaporation. *Eye Contact Lens* 2008; **34**(6)**:** 326-330.

139. Peters K, Millar T. The role of different phospholipids on tear break-up time using a model eye. *Curr Eye Res* 2002; **25**(1)**:** 55-60.

140. Rohit A, Willcox M, Stapleton F. Tear lipid layer and contact lens comfort: a review. *Eye Contact Lens* 2013; **39**(3)**:** 247-253.

141. Henriques M, Sousa C, Lira M, Elisabete M, Oliveira R, Oliveira R *et al.* Adhesion of Pseudomonas aeruginosa and Staphylococcus epidermidis to silicone-hydrogel contact lenses. *Optom Vis Sci* 2005; **82**(6)**:** 446-450.

142. Jones L, Mann A, Evans K, Franklin V, Tighe B. An in vivo comparison of the kinetics of protein and lipid deposition on group II and group IV frequent-replacement contact lenses.

Optom Vis Sci 2000; **77**(10)**:** 503-510.

143. Nichols JJ. Deposition on silicone hydrogel lenses. *Eye Contact Lens* 2013; **39**(1)**:** 20-23.

144. Pucker AD, Nichols JJ. Analysis of meibum and tear lipids. *Ocul Surf* 2012; **10**(4)**:** 230-250.

145. Butovich IA. On the lipid composition of human meibum and tears: comparative analysis of nonpolar lipids. *Invest Ophthalmol Vis Sci* 2008; **49**(9)**:** 3779-3789.

146. Butovich IA, Uchiyama E, McCulley JP. Lipids of human meibum: mass-spectrometric analysis and structural elucidation. *J Lipid Res* 2007; **48**(10)**:** 2220-2235.

147. Rantamaki AH, Seppanen-Laakso T, Oresic M, Jauhiainen M, Holopainen JM. Human tear fluid lipidome: from composition to function. *PLoS One* 2011; **6**(5)**:** e19553.

148. Lorentz H, Heynen M, Kay LM, Dominici CY, Khan W, Ng WW *et al.* Contact lens physical properties and lipid deposition in a novel characterized artificial tear solution. *Mol Vis* 2011; **17:** 3392-3405.

149. Solomon OD, Freeman MI, Boshnick EL, Cannon WM, Dubow BW, Kame RT *et al.* A 3-year prospective study of the clinical performance of daily disposable contact lenses compared with frequent replacement and conventional daily wear contact lenses. *CLAO J* 1996; **22**(4)**:** 250-257.

150. Sanbar SS, Smet G. Hypolipidemic effect of polyvinylpyrrolidone in man. *Circulation* 1968; **38**(4)**:** 771-776.

151. Jones L, Subbaraman L, Rogers R, Dumbleton K. Surface treatment, wetting and modulus of silicone hydrogels. *Optician* 2006; **4**(1)**:** 24-43.

152. Evinger C, Manning KA, Sibony PA. Eyelid Movements - Mechanisms and Normal Data. *Invest Ophthalmol Vis Sci* 1991; **32**(2)**:** 387-400.

153. McDermott AM, Qin G, Baidouri H, Glasser A, Kuether C, Morris CA *et al.* A Biological Model of Contact Lens Wear. *Invest Ophthalmol Vis Sci* 2016; **57:** 1466.

154. Nakano T, Kato M, Morito Y, Itoi S, Kitazawa S. Blink-related momentary activation of the default mode network while viewing videos. *P Natl Acad Sci USA* 2013; **110**(2)**:** 702-706.

155. Malbouisson JM, AA EC, Messias A, Leite LV, Rios GD. Upper and lower eyelid saccades describe a harmonic oscillator function. *Invest Ophthalmol Vis Sci* 2005; **46**(3)**:** 857-862.

156. Ghannam MT, Esmail MN. Rheological properties of poly(dimethylsiloxane). *Ind Eng Chem Res* 1998; **37**(4)**:** 1335-1340.

157. Hiller J, Lipson H. Design and analysis of digital materials for physical 3D voxel printing.

Rapid Prototyping J 2009; **15**(2)**:** 137-149.

158. Kudo K, Ishida J, Syuu G, Sekine Y, Ikeda-Fukazawa T. Structural changes of water in poly(vinyl alcohol) hydrogel during dehydration. *J Chem Phys* 2014; **140**(4)**:** 044909.

159. Bentivoglio AR, Bressman SB, Cassetta E, Carretta D, Tonali P, Albanese A. Analysis of blink rate patterns in normal subjects. *Mov Disord* 1997; **12**(6)**:** 1028-1034.

160. Doughty MJ, Naase T. Further analysis of the human spontaneous eye blink rate by a cluster analysis-based approach to categorize individuals with 'normal' versus 'frequent' eye blink activity. *Eye Contact Lens* 2006; **32**(6)**:** 294-299.

161. Dilly PN. Structure and function of the tear film. *Adv Exp Med Biol* 1994; **350:** 239-247.

162. Guitton D, Simard R, Codere F. Upper eyelid movements measured with a search coil during blinks and vertical saccades. *Invest Ophthalmol Vis Sci* 1991; **32**(13)**:** 3298-3305.

163. Jiang X, Tien G, Huang D, Zheng B, Atkins MS. Capturing and evaluating blinks from video-based eyetrackers. *Behav Res Methods* 2013; **45**(3)**:** 656-663.

164. Kennard DW, Glaser GH. An Analysis of Eyelid Movements. *J Nerv Ment Dis* 1964; **139:** 31-48.

165. Collewijn H, van der Steen J, Steinman RM. Human eye movements associated with blinks and prolonged eyelid closure. *J Neurophysiol* 1985; **54**(1)**:** 11-27.

166. Conrady CD, Joos ZP, Patel BC. Review: The Lacrimal Gland and Its Role in Dry Eye. *J Ophthalmol* 2016; **2016:** 7542929.

167. Tutt R, Bradley A, Begley C, Thibos LN. Optical and visual impact of tear break-up in human eyes. *Invest Ophthalmol Vis Sci* 2000; **41**(13)**:** 4117-4123.

168. Koh S, Higashiura R, Maeda N. Overview of Objective Methods for Assessing Dynamic Changes in Optical Quality. *Eye Contact Lens* 2016; **42**(5)**:** 333-338.

169. Sweeney DF, Millar TJ, Raju SR. Tear film stability: a review. *Exp Eye Res* 2013; **117:** 28-38.

170. Keir N, Jones L. Wettability and silicone hydrogel lenses: a review. *Eye Contact Lens* 2013; **39**(1)**:** 100-108.

171. Mengher LS, Bron AJ, Tonge SR, Gilbert DJ. A non-invasive instrument for clinical assessment of the pre-corneal tear film stability. *Curr Eye Res* 1985; **4**(1)**:** 1-7.

172. Johnson ME, Murphy PJ. The Effect of instilled fluorescein solution volume on the values and repeatability of TBUT measurements. *Cornea* 2005; **24**(7)**:** 811-817.

173. Guillon JP. Non-invasive Tearscope Plus routine for contact lens fitting. *Cont Lens Anterior Eye* 1998; **21 Suppl 1:** S31-40.

174. Elliott M, Fandrich H, Simpson T, Fonn D. Analysis of the repeatability of tear break-up time measurement techniques on asymptomatic subjects before, during and after contact lens wear. *Cont Lens Anterior Eye* 1998; **21**(4)**:** 98-103.

175. Nichols JJ, Nichols KK, Puent B, Saracino M, Mitchell GL. Evaluation of tear film interference patterns and measures of tear break-up time. *Optom Vis Sci* 2002; **79**(6)**:** 363-369.

176. Hirji N, Patel S, Callander M. Human tear film pre-rupture phase time (TP-RPT)--a non-invasive technique for evaluating the pre-corneal tear film using a novel keratometer mire. *Ophthalmic Physiol Opt* 1989; **9**(2)**:** 139-142.

177. Best N, Drury L, Wolffsohn JS. Clinical evaluation of the Oculus Keratograph. *Cont Lens Anterior Eye* 2012; **35**(4)**:** 171-174.

178. Busin M, Wilmanns I, Spitznas M. Automated corneal topography: computerized analysis of photokeratoscope images. *Graefes Arch Clin Exp Ophthalmol* 1989; **227**(3)**:** 230-236.

179. Kojima R, Caroline P, Kinoshita B, Lamps M, Andre M, Rosen C. Applications of Corneal Topography Beyond Corneal Shape. *Contact Lens Spectrum* 2013; **28:** 36-51.

180. Bruce AS, Mainstone JC, Golding TR. Analysis of tear film breakup on Etafilcon A hydrogel lenses. *Biomaterials* 2001; **22**(24)**:** 3249-3256.

181. Read ML, Morgan PB, Kelly JM, Maldonado-Codina C. Dynamic contact angle analysis of silicone hydrogel contact lenses. *J Biomater Appl* 2011; **26**(1)**:** 85-99.

182. Keir N, Woods CA, Dumbleton K, Jones L. Clinical performance of different care systems with silicone hydrogel contact lenses. *Cont Lens Anterior Eye* 2010; **33**(4)**:** 189-195.

183. Paugh JR, Stapleton F, Keay L, Ho A. Tear exchange under hydrogel contact lenses: methodological considerations. *Invest Ophthalmol Vis Sci* 2001; **42**(12)**:** 2813-2820.

184. Lin MC, Soliman GN, Lim VA, Giese ML, Wofford LE, Marmo C *et al.* Scalloped channels enhance tear mixing under hydrogel contact lenses. *Optom Vis Sci* 2006; **83**(12)**:** 874-878.

185. Shaw AJ, Collins MJ, Davis BA, Carney LG. Eyelid pressure and contact with the ocular surface. *Invest Ophthalmol Vis Sci* 2010; **51**(4)**:** 1911-1917.

186. Cong H, Pan T. Microfabrication of conductive PDMS on flexible substrates for biomedical applications. *Nano/Micro Engineered and Molecular Systems* 2009; **4th IEEE International Conference:** 731-734.

187. Nichols KK, Foulks GN, Bron AJ, Glasgow BJ, Dogru M, Tsubota K *et al.* The international

workshop on meibomian gland dysfunction: executive summary. *Invest Ophthalmol Vis Sci* 2011; **52**(4)**:** 1922-1929.

188. Parfitt GJ, Lewis PN, Young RD, Richardson A, Lyons JG, Di Girolamo N *et al.* Renewal of the Holocrine Meibomian Glands by Label-Retaining, Unipotent Epithelial Progenitors. *Stem Cell Reports* 2016; **7**(3)**:** 399-410.

189. Nason RJ, Boshnick EL, Cannon WM, Dubow BW, Freeman MI, Kame RT *et al.* Multisite comparison of contact lens modalities. Daily disposable wear vs. conventional daily wear in successful contact lens wearers. *J Am Optom Assoc* 1994; **65**(11)**:** 774-780.